Genetic Variation in Photosynthetic Responses to Chilling Modulates Proton Motive Force, Cyclic Electron Flow and Photosystem II Photoinhibition.

Donghee Hoh[1,2], Isaac Osei-Bonsu[1], Abhijnan Chattopadhyay[1], Atsuko Kanazawa[1,4], Nicholas Fisher[1], Oliver L Tessmer[1], Jeffrey Cruz[1], Philip A. Roberts[5], Bao-Lam Huynh[5], David Hall[1] and David M. Kramer[1,3*]

Affiliations

[1] MSU DOE Plant Research Laboratory, [2] Department of Cell & Molecular Biology, [3] Department of Biochemistry and Molecular Biology, [4] Department of Chemistry, Michigan State University, East Lansing, MI 48824 USA, [5] Department of Nematology University of California, Riverside CA 92521 USA

*Corresponding Author

Keywords

Photosynthesis, Natural Variation, Quantitative Trait Loci (QTL), Chilling stress (Low temperature stress), Cowpea, Chlorophyll fluorescence, DEPI, MultispeQ

Abstract

The work demonstrates the use of detailed, high-throughput phenotyping to generate and test mechanistic models to explain the genetic diversity of photosynthetic responses to abiotic stress. We assessed a population of recombinant inbred lines (RILs) of cowpea (*Vigna unguiculata.* (L.) Walp.) with significant differences in a range of photosynthetic responses to chilling. We found well-defined, colocalized (overlapping) QTL intervals for photosynthetic parameters, suggesting linkages among the redox states of Q_A, the thylakoid *pmf*, through effects on cyclic electron flow and photodamage to PSII. We propose that these genetic variations optimize photosynthesis in the tolerant lines under low temperatures, preventing recombination reactions within Photosystem II that can lead to deleterious $^1O_2$ production. By contrast, we did not observe linkages to PSI redox state, PSI photodamage or ATP synthase activity, or nyctinastic (diurnally controlled) leaf movements, likely indicating that several proposed models likely do not contribute to the genetic control of photosynthesis at low temperature in our mapping panel. The identified QTL intervals include a range of potential causative genetic components, with direct applications to breeding of photosynthesis for more climate-resilient productivity.

Introduction

Photosynthetic performance is strongly impacted by abiotic stress factors, accounting for substantial losses of sustainable plant productivity, and thus critical for maintaining or expanding sustainable agriculture, particularly in a rapidly changing environment. Because photosynthesis directly contributes to yield, understanding how it performs and is regulated under non-ideal conditions may be the key to improving plant productivity (Zelitch 1982; Long, Zhu, Naidu & Ort 2006; Raines 2011). Stress resistance traits are thus the target of intensive efforts at breeding or engineering more robust plant responses. However, the important effects may include complex, rapidly fluctuating combinations of temperature, water availability, light intensity etc. that are not typically seen under controlled laboratory conditions (Tikkanen *et al.* 2012; Cruz *et al.* 2016). Plants have adapted to meet the challenges of specific environments, and it may be possible to harness this biodiversity to improve crop performance in changing environments (Lawson et al. 2012). However, such traits may not be present in our current crops or well-studied model systems. Thus, discovering the mechanistic bases of useful or adaptive photosynthetic traits will require exploration of wider ranges of genotypes and environmental conditions.

Chilling (or suboptimal) temperatures are often major constraints on photosynthesis, productivity, and geographical distribution of important cultivated crops (Allen & Ort 2001). Counterintuitively, transient chilling (sub-optimal, but non-freezing temperatures) can be a major problem even with global climate change, which induces not only warming but variations in temperatures, leading to unpredictable periods of increased and decreased growth temperatures (Gu *et al.* 2008). Multiple components of photosynthesis can be affected by chilling, including thylakoid electron transport, carbon fixation, stomatal conductance, regulation of gene expression (Allen & Ort 2001). Key steps in the light reactions have also been suggested to be the primary limitations under chilling, e.g. thylakoid electron transport, photodamage and repair of photosystem II (PSII) (Aro, Virgin & Andersson 1993; Moon, Higashi, Gombos & Murata 1995), photosystem I (PSI) (Sonoike 1996), activation of alternative electron sinks (Ivanov *et al.* 2012) and oxidative stress (Sassenrath, Ort & Portis Jr 1990; Hutchison, Groom & Ort 2000). The primary limitations may be specific to differences in species, genotypes, developmental stages or other environmental conditions.

The increasing sophistication of high-throughput photosynthetic phenotyping, combined with powerful genetic approaches and biochemical methods, enables us to test for interactions among natural specific mechanisms that may underlie genetic variations in tolerance to low temperatures. This can be achieved by identifying statistical associations between measured traits with genetic polymorphisms in a panel or library of genetically-diverse lines (Broman 2001). Quantitative Trait Loci (QTL) and genome wide association studies (GWAS) have been extensively used by plant breeders to identify genetic markers for desirable traits that can be used to develop introgression of these multiple traits into elite production lines

of crop (Boukar, Fatokun, Huynh, Roberts & Close 2016). For example, bulk or aggregated phenotypes based on the data such as yield or disease resistance were targeted for most QTL analyses (Muchero *et al.* 2013; Huynh *et al.* 2016). It has been much more difficult to identify specific, causative genetic loci associated with QTLs (Roff 2007; Baxter 2020), largely because of the low genomic resolution of the methods (Miles & Wayne 2008).

In this work, we focus on discovering and testing possible mechanistic bases of such variations by assessing cosegregation (or lack thereof) between genetic diversity and multiple traits. To achieve this, we took advantage of recently developed high-throughput phenotyping tools that can measure multiple, mechanistically-related, photosynthetic phenotypes under simulated, field-like environmental conditions (Cruz *et al.* 2016; Kuhlgert *et al.* 2016). We then compared the QTL profiles for the different phenotypes to assess whether the genetic diversity in one process is linked to that of others.

The phenotyping tools used in this work can make time-resolved, semi-simultaneous, measurements of photosynthetic processes in many genotypes. By testing for possible co-associations between genetic components and various phenotypes, it is possible to assess if variations in processes are genetically or mechanistically linked. Here, we use the term "linked" broadly to mean that processes are either controlled by the same genetic locus or mechanistically connected so that one process impacts the other. In this context, the observation that QTLs for two phenotypes do *not* overlap, would indicate that genetic diversity controlling one process is not measurably controlling the other, at least in the specific population and experimental conditions. In other words, a linkage *could* exist in another population or under different conditions. On the other hand, observing strongly overlapping QTLs can be considered as evidence for genetic or mechanistic linkages, but with the following important caveats: 1) With most diversity panels, there are likely to be many gene polymorphisms under a single QTL, and one cannot exclude the possibility that two processes are influenced by two distinct loci within the statistical resolution of the QTL. 2) Traits may be impacted by a large number of weak linkages, each making only a small impact, and thus may not appear as distinct QTL. Here, we consider only those variations that do show significant associations, implying that a limited number of discrete genetic components measurably affect on a phenotype, and thus one can make (careful) inferences about how they are linked to others. 3) One trait may affect the ability to measure another even though they are not directly functionally linked. For instance, traits that affect the optical properties of a leaf, e.g. leaf thickness, accumulation of anthocyanins etc. may decrease the sensitivity of the measurement of a phenotype so that the phenotype may appear to have a linkage with these traits. This issue above may be particularly important for measurements made using the same basic techniques. For example, a number of our measurements are made using saturation pulse fluorescence kinetics so that artifacts in one measurement may become evident in the others (see (Baker, Harbinson & Kramer 2007)), giving rise to apparent linkages. However, as discussed in Results, the fact that QTL for these various parameters are conditionally linked, argues against these types of effects in the current data set. 4) It is also possible that the effects of one process

may be canceled out by others, masking an effect. This may be expected for homeostatic processes, e.g., where the network of regulatory processes results in compensatory (e.g., feedback and feedforward) regulation. In these cases, effects on some parameters may only be observed when the compensatory homeostatic mechanisms fail. 5) Phenotypes can be linked through indirect and time-dependent intermediates.

Specifically, we explored natural variations in chilling tolerance on photosynthesis in *Vigna unguiculata* (cowpea), a warm-climate species with a high level of genetic diversity and significant variable phenotypic responses to abiotic stress among its cultivars (Huynh *et al.* 2018). We demonstrate strong, genotype-dependent effects of chilling on the primary reactions of photosynthesis that likely involve the network that co-regulates the light and assimilatory reactions of photosynthesis. This network involves the establishment of the thylakoid proton motive force (*pmf*) and subsequent acidification of the thylakoid lumen, which activates the qE response and the "photosynthetic control" of electron flow at the level of the cytochrome b_6f complex (Avenson et al. 2005). The results show qualitatively similar effects, supporting causative linkages.

Material and Methods

Plant materials

Cowpea recombinant inbred lines (RILs) used for QTL mapping were selected by the pre-screening of nine pairs of RIL parental lines (Table S1). This population consisted of 90 RILs (F10 generation) originating from a cross between cultivar California Blackeye 27 (CB27) bred by the University of California (UC), Riverside (Ehlers, Hall, Patel, Roberts & Matthews 2000) and breeding line 24-125B-1 developed by Institute de Recherche Agricole pour le Développement (IRAD, Cameroon).

Growth and Experimental conditions

Cowpea seeds were planted in Suremix (Michigan Grower Products Inc, USA) with half-strength Hoagland's nutrient solution and germinated under a 14hr: 10hr day: night cycle with a daylight intensity of 500 μmol photons m^{-2} s^{-1} and temperatures of 29 °C/19°C (day/night), 60% relative humidity in growth chambers (BioChambers, Winnipeg, Canada). Seedlings were then transferred to DEPI chambers and allowed to acclimate for one day under growth light and temperature conditions. Imaging of chlorophyll fluorescence parameters was initiated on subsequent days as the light intensity was changed every 30 minutes with a 10/14 hour light/dark pattern based on a sinusoidal curve and a peak intensity of 500 μmol photons m^{-2} s^{-1} (Figure S1), imitating a cloudless sunny day. On Day 2, For chilling treatment day/night temperatures were shifted to 19 °C/13°C on the second day of imaging. The temperatures were selected

based on average field conditions from 2012 to 2016 in Tulare, Central valley of California where cowpea is normally grown in April one month ahead of normal planting. Data is from National Oceanic and Atmospheric Administration, https://www.noaa.gov (Table S2). Detailed experimental information for the temperature and relevant time points are referred to Table S3.

Photosynthetic phenotyping

Chlorophyll fluorescence imaging was performed using Dynamic Environmental Phenotype Imager (DEPI) chambers (Cruz et al., 2016), with modifications described in (Tietz, Hall, Cruz & Kramer 2017) . Fluorescence images were captured in fully dark-adapted plants and at different times following illumination to obtain estimates of photosynthetic parameters using the methods described in (Baker & Oxborough 2004; Baker *et al.* 2007; Tietz *et al.* 2017). Values for steady-state F (F_S) and with oxidized Q_A (F_0'), or following short (~6s) dark period with far-red illumination to obtain estimates of F_0', or 1 min dark periods to obtain F_M'' values to estimate rapidly (q_E) and slowly (q_I and q_Z) relaxing contributions to NPQ. Images of maximum fluorescence yields with Q_A was fully reduced (F_M', F_M'') were collected after ~0.3 s of saturating white light (~10,000 µmol m^{-2} s^{-1}), while those of F_0' and F_0'' were collected immediately after 6 seconds of far-red illumination (approximately ~4.6 µmol m^{-2} s^{-1})). During the period of sinusoidal illumination, photosynthetic phenotyping was obtained two times per hour. Images of the steady-state (Φ_{II}) PSII quantum yields were derived from images of F_S and F_M' using previously reported methods (Cruz *et al.* 2016). Established methods for non-photochemical quenching use F_M and F_0 images at the beginning of the day. Because of large heliotropic movements of cowpea leaves, alternative equations (Tietz *et al.* 2017) were used for generating images of non-photochemical quenching (NPQt), photoinhibition-related quenching (qIt), energy-dependent quenching (qEt) and Q_A redox state PSII center opened (q_L). All image processing was performed using software (Visual Phenomics 5, https://caapp-msu.bitbucket.io/projects/visualphenomics5.0/) developed in-house in JAVA (Netbeans, link) and based on the open-source Fiji API (https://imagej.net/Fiji). Fluorescence and absorbance measurements were also performed using the hand-held MultispeQ V2.0, based on that described previously (Kuhlgert *et al.* 2016). To account for variations in leaf chlorophyll content, the light-induced thylakoid *pmf*, as estimated by the ECSt parameter (Baker *et al.* 2007) was normalized to relative chlorophyll content (ECSt/(SPAD value)).

Linkage analysis and QTL mapping

Single nucleotide polymorphism (SNP) markers of genotype data of CB27 x 24-125B-1 were obtained from (Lonardi *et al.* 2019), based on EST sequences produced by (Muchero *et al.* 2009; Lucas *et al.* 2011). IciMapping 4.1 (http://www.isbreeding.net) was used for construction of the initial linkage-map (Meng, Li, Zhang & Wang 2015), but this was followed by Rqtl segregation analysis, as described below.

Redundant markers were removed using the IciMapping "BIN' function before constructing the linkage map. The linkage map was constructed using the Kosambi function using its RECORD ordering algorithm (Van Os, Stam, Visser & Van Eck 2005), then aligned against the cowpea consensus genetic map (Huynh *et al.* 2016). For comparisons, QTL analysis was also performed using Multiple QTL Mapping (MQM) model (genome scan with multiple QTL models), introduced by Ritsert Jansen initially (Jansen 2004), as implemented in the Rqtl package (Broman & Sen 2009). The Rqtl fill.geno function, which is based on a Hidden Markov Model, was used to fill in missing genotypic data. Levels of significance were determined using a permutation analysis implemented with the Rqtl mqmpermutation and mqmscan functions, over all replicates, and with the number of permutations set at 1000 and a nominal significance cutoff of $p < 0.05$. Candidate genes in the QTL intervals were predicted by pseudomolecules (http://harvest-web.org) through BLAST in early release genomes in Phytozome (www.phytozome.net/) and those are annotated by Pfam, Panther, EuKaryotic Orthologous Groups (KOG), Kyoto Encyclopedia of Genes and Genomes (KO), Gene Ontology (GO) and best-hit of *Arabidopsis* gene.

Lincomycin treatment

For lincomycin experiments, detached leaves are vacuum infiltrated with 0.2 g/L lincomycin hydrochloride until full inundation of cells by the solution. The control plants were vacuum infiltrated with deionized water (DI) with the same procedure. To avoid dryness of leaves, infiltrated leaves were floated in plates with either lincomycin solution or DI water. Following infiltration, plates containing leaves and solution were kept under low light (50 µmol, m^{-2}, s^{-1}) for 20 min and then dark-adapted 20 min for measuring initial maximal PSII quantum efficiency (Fv/Fm). After that, Fv/Fm measurements were followed by 1hr of high light (HL) (1000 µmol, m^{-2}, s^{-1}) and 20 min dark adaptation to dissipate qE in the DEPI chamber. For the low temperature treatment (LT), the temperature was decreased from 29°C to 19°C and 10°C every two hours of HL treatment (Figure S2).

Quantification of nyctinastic leaf movements (NLM)

Qualitative measurements of nyctinastic leaf movement (NLM) values were obtained by measuring relative changes in the projected leaf tip-to-petiole distances of the time-resolved plant fluorescence images. Fluorescence images were taken during saturation pulses (i.e. which were used to estimate F_M"), which showed the strongest contrast against background interference. Each image was thresholded to separate the leaf area from the background using the triangle thresholding algorithm (Zack, Rogers & Latt 1977) which accounts for vignetting effects of the cameras. The image regions for each plant were determined automatically by the code but verified manually, and the tip-to-petiole distance taken as the

long axis of a rectangle fitted to the projected leaf image. To account for differences in leaf morphology and size, fractional changes peak-to-peak distance normalizing to that of the presumed fully expanded leaf states taken at midday.

Results and Discussion

Dynamic photosynthetic phenotyping of the RIL population

Figure 1 shows heat maps representing the time- and genotype-dependencies of photosynthetic parameters (Φ_{II}, NPQt, qEt, qIt and qL) obtained from DEPI over the three days of the experiment, for control (Panels A-E) and chilling (F-J) treatments. Each row in Figure 1 represents the averaged responses (n≥4) for individual genotypes. The rows were ordered based on the average values of Φ_{II} taken on Day 3 (the second day of chilling). The blue and red rectangles represent the 24-125B-1 and CB27 respectively. Color legends for both conditions are set to the same to compare two conditions. For all parameters, significant changes in the low temperature compared to control conditions are shown in Figure S3.
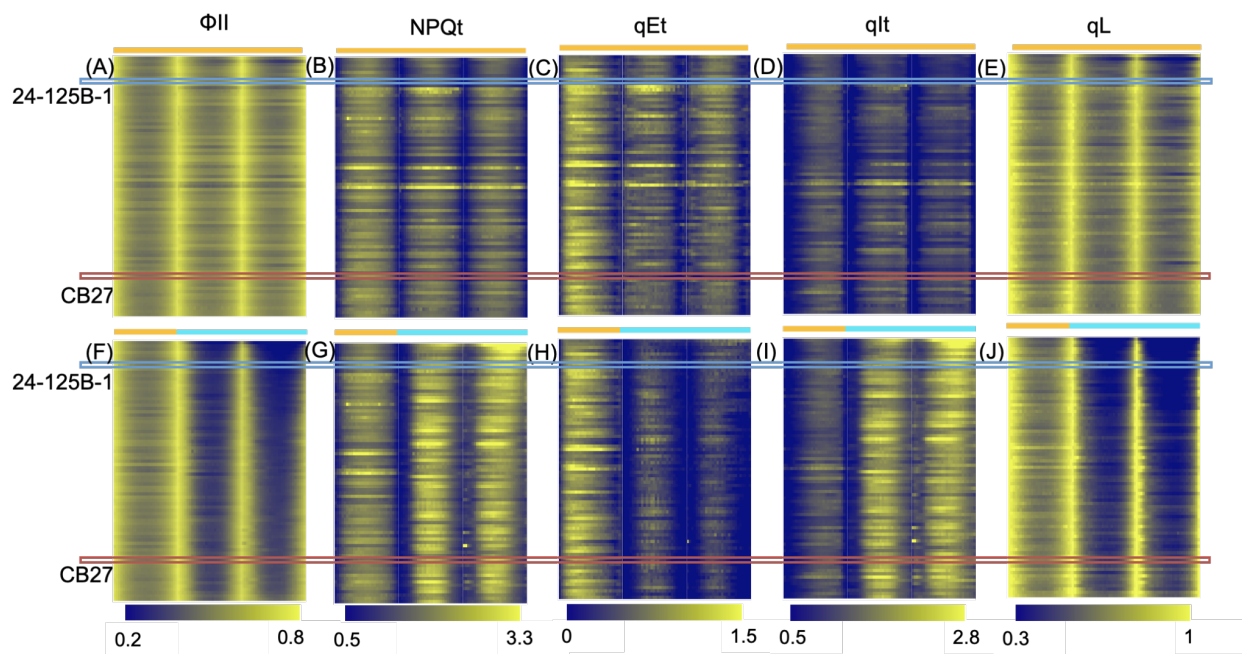

Figure 1. High-throughput photosynthetic phenotyping of recombinant lines (RILs) in DEPI chambers under control and low temperatures. Photosynthetic phenotyping of the CB27 x 24-125B-1 RIL population was performed in a DEPI chamber on five-day-old seedlings over three days. Low (chilling) temperatures were imposed on the second day of imaging under sinusoidal light. Heat maps produced using the OLIVER program (Tessmer et al. 2018) show measured (non-normalized) averaged replicate values over the RIL population (n≥4). Each row represents average values for a different

genotype. The blue and red rectangles represent the 24-125B-1 and CB27 respectively. The remaining rows represent individual genotypes over the RIL population. Five photosynthetic parameters were collected by the DEPI chamber during the day, upper panels are control conditions (A-E) and lower panels (F-J) are under chilling conditions. Each row in Figure 1 represents the averaged responses (n≥4) for each genotype. The rows were ordered based on the average values of Φ_{II} taken on Day 3 (the second day of chilling). Color legends for both conditions are set to the same to compare two conditions.

On Day 1, under the control temperature, we observed relatively small variations in Φ_{II} between genotypes and between the first and subsequent days of exposure to the sinusoidal illumination (Fig. 1, panel A). For each line, Φ_{II} values tended to be high in the morning, decrease towards midday near peak PAR, and essentially fully recover by the end of the day. These patterns indicate that higher PAR levels towards midday partially saturated photosynthesis, but did not induce long-lasting photodamage. Consistent with this interpretation, total NPQt was low in the morning, highest at about midday and fully recovered at the end of illumination. Similar patterns were also seen for the qEt and qIt components of NPQ. Some genotypes showed noticeably larger NPQt values throughout the experiment (e.g. genotypes SRIL-006, SRIL-039, SRIL-105) and these increases could be attributed mainly to increased qEt (compare Figs. 1B and 1C).

Compared to Day 1, measurements under the lower temperatures on Days 2 and 3 showed differences from CT (Fig. 1 Panels F-J), with lower Φ_{II} values and higher NPQt values, consistent with decreases in productive energy transduction and increases in energy dissipation through NPQ. There were also larger genotype-dependent variations in photosynthetic parameters. In general, we observed a trade-off between fast and slowly relaxing forms of NPQ, with the extent of the rapidly-reversible qEt component of NPQ decreased while that of the more slowly reversible components increased. By contrast with CT, Φ_{II} (Fig. 1F), NPQt (Fig. 1G) and qIt (Fig. 1I) values failed to recover at the end of illumination, suggesting that low temperature-induced substantial photoinhibition, photodamage or other long-lasting quenching processes. Another striking feature was the strong decrease in qL during the low temperature treatments, reflecting a more reduced Q_A redox state, after chilling stress (Fig.1J), most likely reflecting temperature-dependent decreases in the rates of oxidation of Q_A- that are not compensated by increases in NPQ.

Figure S4 shows histograms of the photosynthetic parameters taken at the middle of the third day of the experiment, at highest light intensity, 500 μmol m^{-2} s^{-1}, under control and low temperature conditions. Going from control to low temperature on Day 2, Φ_{II}, qL and qEt decreased, while NPQt and qIt increased. Overall, the distributions of values for each parameter across genotypes were substantially larger under the low temperature compared to the control, suggesting the appearance of larger variations in low temperature response traits. The distributions of values substantially exceeded those between the two parental lines, suggesting partial transgressive segregation of traits.

Quantitative Trait Loci (QTL) for photosynthetic parameters show shifting control of photosynthetic processes with stress

The figure 2 shows logarithm of the odds (LOD) score plots of photosynthetic data for a selected time point at 1.5 hr prior to the end of Day 3 (206 µmol m^{-2} s^{-1}) , i.e. quantitative trait loci (QTL) for the data in Fig. 1. We observed several distinct intervals for each photosynthetic phenotype and co-association of intervals on Chrs 4 and 9 (as discussed below). Time courses of LOD score plots are in Fig. 3 and S5.

To refer to specific intervals related to different conditions and phenotypes, we established a standard nomenclature to allow comparisons of QTLs that appeared for different parameters, conditions and times that follow the format described in the following:

Chromosome number - Index - Phenotype - Temperature

where control and low temperature are abbreviated as CT and LT. The indexes are numbered with Arabic numerals in the order of genomic loci of identified QTLs in each chromosome for the QTLs for that phenotype. Table S4. summarizes the name, genomic locations, flanking markers and conditions for each QTL. It is important to note that, while we assigned names for apparently overlapping regions of significant associations, multiple causative polymorphisms may underlie these regions, as discussed below. It is also noteworthy that the parameters measured by DEPI were all based on analysis of chlorophyll fluorescence and thus systematic artifacts in measurements could affect all parameters. However, the facts that the individual parameters show distinct patterns over time, and that similar patterns appeared in completely independent parameters, obtained with the MultispeQ instrument (below) further substantiates our interpretation that they reflect different (but interacting) processes.
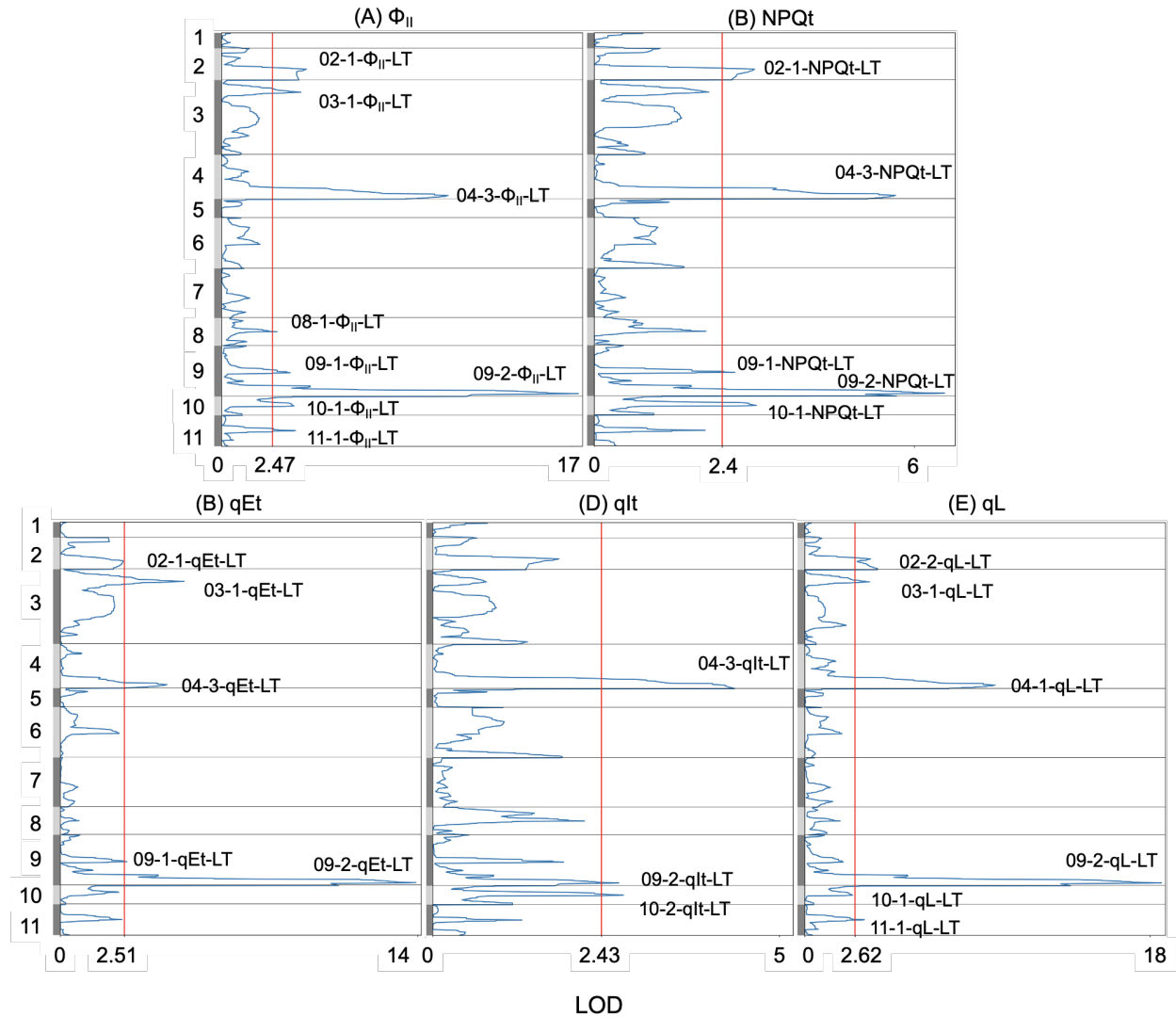
Figure 2. QTL analysis of photosynthetic parameters from DEPI in the low temperature condition. Logarithm of odds (LOD) score plots of photosynthetic data (A, Φ_{II}; B, NPQt; C, qEt; D,qlt ; E;qL) from DEPI in the LT condition measured at 1.5 hr prior to the end of Day 3 (206 µmol m^{-2} s^{-1}). The genetic position is indicated by the y-axis. LOD scores above statistical thresholds, determined by permutation analysis as described in Materials and Methods, are indicated by the red lines. The index is numbered with Arabic numerals in the order of genomic loci in each Chr for the QTLs for that phenotype.

Figure 3 shows a time course for statistical associations between genetic markers and photosynthetic parameters. The results are plotted as heat maps with color indicating the log of odds (LOD) scores for the association of phenotypic differences with genomic markers. Distinct patterns of QTL were observed for each control day and chilling treatment days, as well as over the time course of each day.
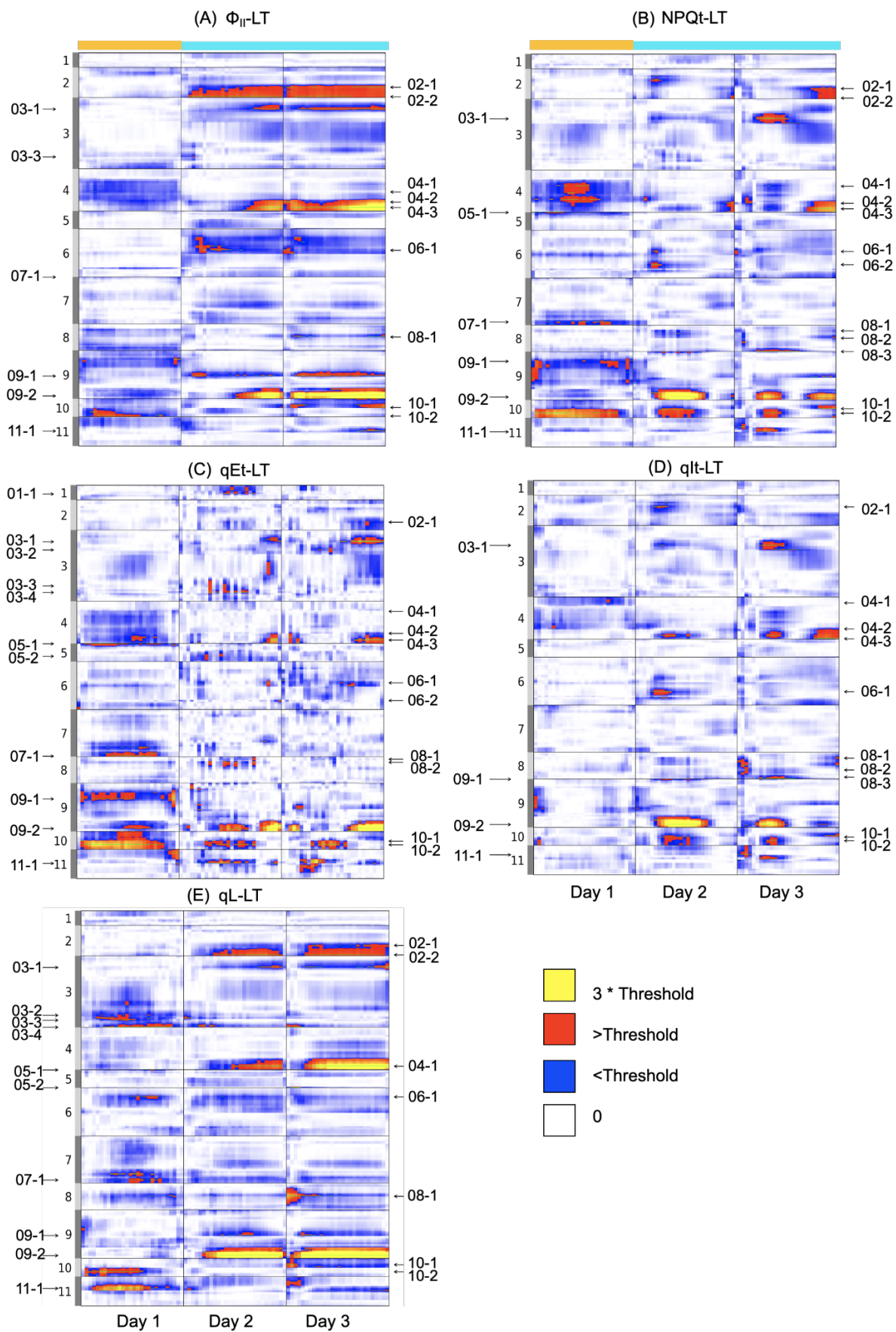
10

(A) Φ_II-LT

(B) NPQt-LT

(C) qEt-LT

(D) qIt-LT

(E) qL-LT

3 * Threshold

>Threshold

<Threshold

0

Figure 3. Time-resolved QTL associations for five photosynthetic parameters (A, Φ_{II}; B, NPQt; C, qEt; D, qlt; E, qL) from DEPI chamber experiments for the CB27 x 24-125B-1 RIL population. The logarithm of odds scores (LOD) score through the time represented as heat maps. The time is indicated on the x-axis and the genetic position is indicated on the y-axis. Day 1 was taken under the control temperature (29°C/19°C, day/night temperatures, orange bar), and the following days were conducted under chilling conditions (19°C/13C°day/night temperature, blue bars). The light intensities (photosynthetically active radiation, PAR) patterns and temperatures are shown above each column of panels. The heat map colors indicate the LOD score as indicated in the legend to the upper right of the panels. LOD scores above statistical thresholds, determined by permutation analysis as described in Materials and Methods, are indicated by red coloration. The apparent local peaks for QTL intervals are indicated by green lines. Each apparent QTL region is labeled according to the naming scheme described in the main text, as chromosome- index- phenotypes- temperature condition (low temperature, LT). The index is numbered with Arabic numerals in the order of genomic loci in each Chr for the QTLs for that phenotype.

On Day 1, two significant QTL intervals were observed for Φ_{II} and qlt (Chr 10), but more intervals were observed for NPQt, qEt and qL (Chrs 3, 4, 5, 6, 7, 9, 10 and 11). As discussed below, some of the intervals overlapped those for different parameters and/or different time points, while others did not. The LOD scores for these intervals changed throughout the day with different patterns. For example, a QTL region for Φ_{II} on Chr 10 (10-2-Φ_{II}-CT/LT) appeared stronger in the morning, but decreased at later times, whereas a interval for qlt on 10 (10-2-qlt-CT/LT) appeared transiently at about the second time point of the day. Other QTLs appeared more constantly over the day, e.g. the intervals for NPQt and qEt on Chrs 7 and 10.

On Day 2, the first day of chilling, a distinct set of QTLs and temporal patterns appeared. While a subset of QTL were carried over from Day 1 (Chr 3 for qL and chr 10 for NPQt, qEt and qlt), some intervals disappeared, e.g. Φ_{II} and qL (e.g. 10-2-Φ_{II}-LT and 10-1-qL-LT on Chr 10), while new intervals appeared, e.g. for Φ_{II} and qL on Chr 2 (02-1,2-Φ_{II}-LT and 02-1,2-qL-LT). These changes in QTL patterns were not seen in the control experiments (Fig. S5), where the temperature of the chamber was not decreased, indicating that they represent temperature-specific genetic effects. Some of the new intervals appeared at very early time points compared to other parameters (e.g. qEt-04-3-LT and qEt-09-2-LT), suggesting that they represent initial effects of low temperature, while others emerged at later times, suggesting they reflect the accumulation of effects under low temperature.

Most of those QTLs found on Day 2 (Φ_{II}, NPQt and qEt on Chrs 2, 4, 6 and 9), were also observed on Day 3, at least at some time points. However, some intervals disappeared (e.g. qEt on Chrs 1, 3, 5 and 8), while new intervals (e.g. NPQt on Chr 11) appeared.

The data in Figures 1 and S4 and 4 show that distinct sets of polymorphisms appear to modulate photosynthetic control mechanisms under different conditions. This type of behavior has been previously observed (e.g., (Flood, Harbinson & Aarts 2011; Prinzenberg, Campos-Dominguez, Kruijer, Harbinson &

Aarts 2020), and can be attributed to the imposition of different, genetically-controlled limitations or regulatory mechanisms under different conditions. The patterns of QTLs change over the course of the experiment, indicating that, under different conditions, distinct sets of genetic components contribute to changes in the control and regulation of photosynthesis. In one example, under CT, fewer intervals were observed under low PAR, where photosynthesis is likely to be light-limited, and a larger, distinct set of intervals appeared under higher light (e.g. 09-2-Φ_{II}-CT, 09-2-qEt-CT and 09-1-qlt-CT), where we expect more processes to limit photosynthesis.

Going from the CT to LT on Day 2, we observed a loss of some QTL intervals, e.g. Φ_{II} and qL (e.g. 10-1-Φ_{II}-LT and 10-1-qL-LT on Chr 10), and the appearance of a larger number of distinct QTL across the various parameters (Fig. 2, 02-1,2-Φ_{II}-LT and 02-1,2-qL-LT). This result is consistent with the observed higher variability of parameters across the population for the various parameters (Fig. S4), suggesting additional impact of genetic components under the non-ideal conditions. Some of the new QTL intervals appeared at very early time points compared to other parameters (e.g. 04-3-qEt-LT and 09-2-qEt-LT), suggesting that they represent initial effects of low temperature, while others emerged at later times, suggesting they reflect the accumulation of effects under low temperature. Overall, these behaviors point to a stress-related shift from one set of processes that is relatively insensitive to the genetic diversity in the panel, to another set that is more strongly impacted by genetic differences.

Co-association of genomic associations reveal potential genetic and mechanistic control networks

As can be seen by comparing the lod plots in Fig 2 and heat maps in Fig. 3, the photosynthetic parameters showed apparent overlaps (co-segregation) with several photosynthetic parameters, consistent with the known interactions among the processes that underlie the measurements. For instance, increasing NPQ often results in a decrease in Φ_{II}, so one may expect apparent linkages. However, as will be seen below, the cases where linkages are not observed, or where the effect directions are not as expected, can be quite informative about possible mechanisms. Note that LOD scores reflect the statistical association rather than effect size, so noisy data can also impact the appearance of a QTL. However, we confirm, below, that the effect sizes show similar behaviors.

Figure 4 summarizes the appearance of overlapping QTLs for the strongest QTL intervals for photosynthetic parameters on Chrs 4, 9 and 8. Different combinations of overlapping QTLs for the various photosynthetic processes appeared at different time points under both control and chilling stress (Fig. 4). The time course of these connections may, to some extent, reflect the sequence of events that leads to the eventual aggregate phenotypes, as discussed in more detail below.

On Day 2, overlapping QTLs appeared on Chr 4 and 9 (04-2/3-Φ_{II}-CT, 04-3-qEt-CT, 04-1-qL-CT, 09-2-Φ_{II}-

13

CT, 09-2-qEt-CT, 09-2-qL-CT, 04-2/3-Φ_{II}-LT, 04-2/3-qEt-LT, 04-1-qL-LT, 09-2-Φ_{II}-LT, 09-2-qEt-LT, 09-2-qL-LT) for Φ_{II}, qEt and qL under both CT and LT conditions, suggesting that these loci impacted photosynthesis under both conditions (Fig. 4 A-B and D-E). The intervals for qEt and qL appeared earlier than those for the other parameters. This trend was more pronounced at LT compared to CT, where the intervals for qEt and qL appeared substantially earlier at LT, suggesting that genetic variations affected the early onset of the photoprotection with subsequent impact on Q_A redox state.

The most striking differences between CT and LT in the Chr 4 and 9 intervals were the impact on NPQt and qIt. CT induced only a short, transient interval for qIt on Chr 4 in the morning (Fig. 4A) and none on Chr 9 (Fig. 4B). By contrast, under LT, qIt-related intervals appeared on both Days 2 and 3 soon after the onset of illumination and persisted for most of Day 2 (Fig. 4D-E), showing temperature-induced photoinhibition. Similar results were seen for Day 3, with the notable exception that the intervals for NPQt and qIt persisted over longer time periods.

The interval on Chr 8 (08-1-Φ_{II}-LT, 08-2-NPQt-LT, 08-2-qIt-LT and 08-1-qL-LT) showed LT-specific effects, but these were predominantly restricted to the morning and evening of Day 3, when light levels were low, indicating that this interval may be associated with longer-term effects, e.g. accumulated photodamage, repair or acclimation responses.

Overall, these results suggest a model where the photosynthetic responses are qualitatively affected by Chrs 4 and 9 loci under both conditions, but with stronger impacts under LT, giving rise to long-lived forms of NPQ, likely reflecting the accumulation of photodamage to PSII. Further, a locus under the intervals on Chr 8 may modulate the response to LT on photoinhibition over longer time periods.
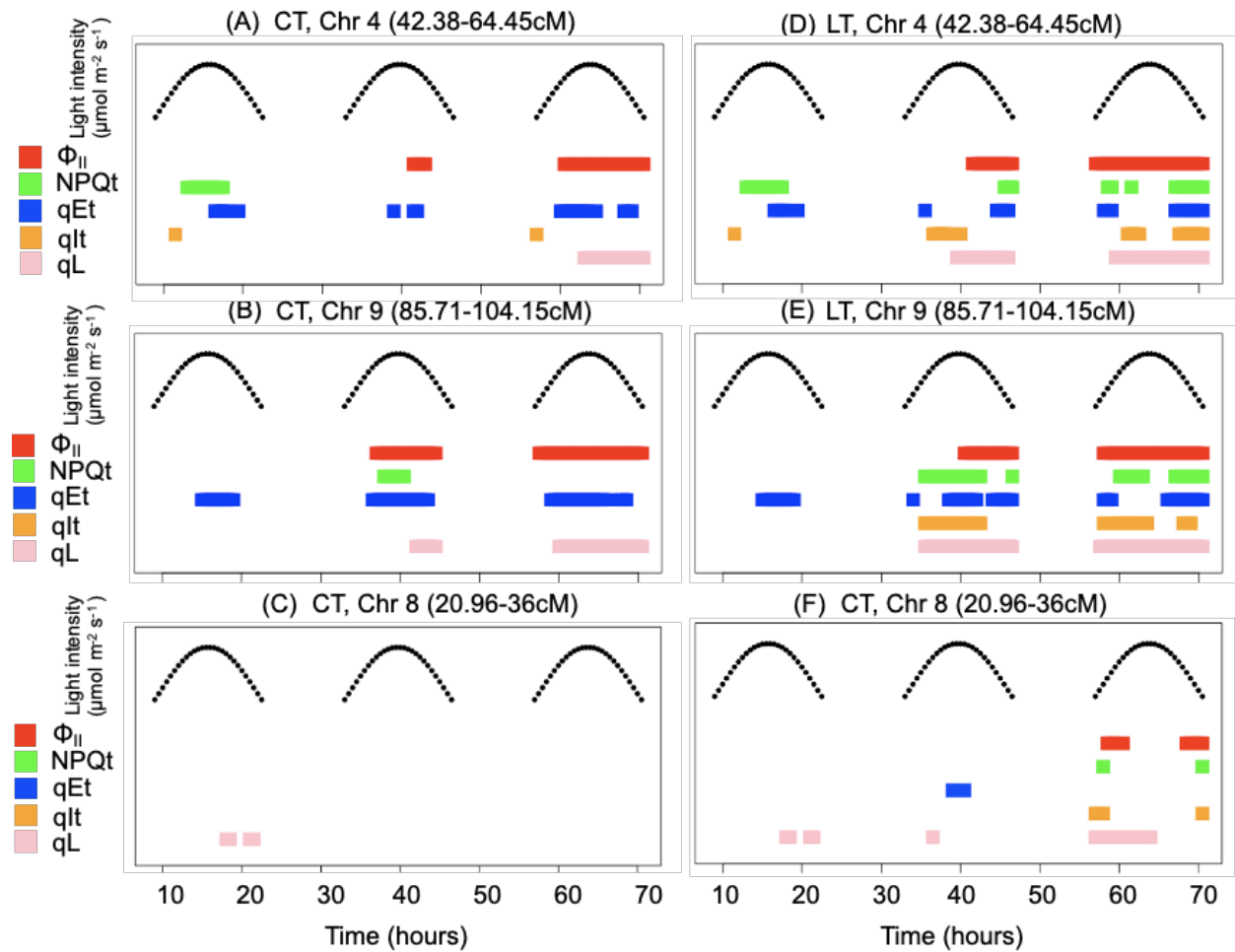
Figure 4. Time course for the appearance and disappearance of the QTLs of five photosynthetic parameters in the selected three loci, Chrs 4, 9 and 8. The appearance and disappearance of the QTLs for three selected loci, Chr 4 42.38-64.45cM (A and D), Chr 9 85.71-104.15 cM (B and E) and chr 8 20.96-36cM (C and F). Conditions were as in Figure 1. The time course for photosynthetically active radiation (PAR) is shown in the upper part of each panel. The presence of significant QTL intervals at the respective positions for each phenotype are shown as filled rectangles with different colors: Φ_{II}, red; NPQt, green; qEt, blue; qlt, orange; qL.

Time-resolved MultispeQ measurements for two parental lines

Figure 5 shows more detailed photosynthetic measurements made using the MultispeQ instrument taken for the parent lines under the same conditions as the experiment in Fig. 1. To avoid disturbing the plants, only 5 measurements were made per day, at the times indicated in Fig. 5. In general, measurements made with both DEPI and MultispeQ showed similar trends. On Day 1, no (or only small) differences were seen between CB27 and 24-125B-1 for all MultispeQ phenotypes, but significant differences emerged under LT treatment on Days 2 and 3.

Compared to CB27, 24-125B-1 showed decreased Φ_{II} (Fig. 5A), increased NPQt (Fig. 5B) and decreased qL (Fig. 5C). These effects were accompanied by significantly higher ECSt, particularly at the beginning of days 2 and 3 (Fig. 5D), indicating a larger thylakoid *pmf*. However, the thylakoid proton conductivity, *g*H+, was either not significantly different, or differed by only small amounts (Fig. 5E), implying that the increased *pmf* in the sensitive line could not be explained by slowing of ATP synthase activity. The light-driven protons flux, estimated by the *v*H+ parameter, was increased in the sensitive line, particularly at the beginning of Day 2, suggesting that the increased *pmf* was related to elevated proton fluxes (Fig. 5F). The ratio of *v*H+/LEF can be used as an indicator of contributions to proton flux from CEF and LEF (Baker *et al.* 2007). In the absence of CEF, we expect a constant *v*H+/LEF because LEF should translocate a constant 3 H+/e-. Engagement of CEF should result in increased *v*H+/LEF. As shown in Fig. 5I, we observed periods of higher *v*H+/LEF, indicating that CEF likely contributed to the observed elevated *pmf* in 24-125B-1 throughout Day 2 and the beginning of Day 3 and Day 4. We observed significantly increased levels of oxidized $P_{700}+$ in 24-125B-1 on Day 3 (Fig. 5G), accompanied by the decreased rate constant for $P_{700}+$ re-reduction (k_{b6f}, Fig. 5H), consistent with a larger photosynthetic control imposed by the higher *pmf*.
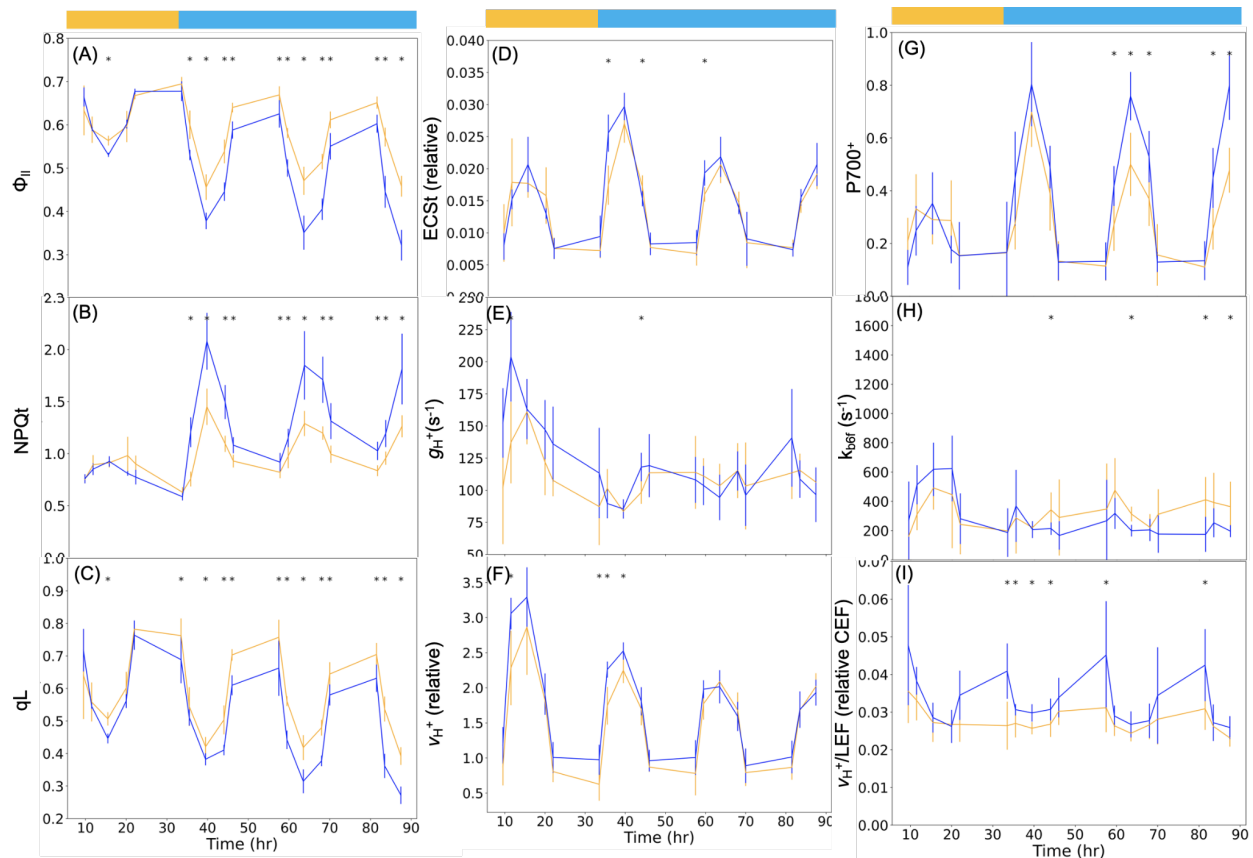
Figure 5. Time-resolved MultispeQ measurements of two parental lines at low temperature. (A, Φ_{II}; B, NPQt; C, qL; D, ECSt (*pmf*); E; *g*H+ , F; *v*H+, G: $P_{700}+$; H; k_{b6f}, I; *v*H+/LEF (relative CEF))
Day 1 was taken under the control temperature (CT, 29°C/19°C day/night temperatures, orange bar and the following days were conducted under low temperature (LT, 19°C/13C°day/night temperature, blue bars). The light intensities (photosynthetically active radiation, PAR) patterns and temperatures are shown above each column of panels. The measurements were taken at five light intensities on Day 1 to 3, following a sinusoidal pattern, 103, 301, 500, 301 and 103 µmol m^{-2} s^{-1}(0.5, 2.5, 6.5, 11 and 13 hr after illumination). On Day 4, three measurements are done at 103, 301, 500 µmol m^{-2} s^{-1} (0.5, 2.5 and 6.5 hr after illumination). The averaged response of n≥4 biological replicates (n≥4) for each photosynthetic phenotype value of two parental lines are shown as orange for CB27 and blue for 24-125B-1. The significant differences between two parental lines by t-test at each point are shown as asterisks at top of the plot (p<0.05).

Detailed phenotyping of the entire RIL population using MultispeQ instruments.

To explore potential underlying genetic connections, we performed measurements across the entire RIL population using MultispeQ instruments. Because MultispeQ measurements require clamping of individual leaves, measurements were made at a selected time and conditions at control and low temperature conditions at the middle of the third day of chilling treatment (highest light intensity), and thus represent both acute and acclimatory responses to the different conditions.

As with the DEPI results (Figs. S4 A-F), LT resulted in decreases (compared to CT) in the average Φ_{II} (Fig. S6A) and increases in average NPQt (Fig. S6B); the distributions of both parameters broadened at low temperature, indicating larger diversity in photosynthetic responses under environmental stress, as also seen for the DEPI results (Fig. S4). The average qL values were increased compared to the DEPI and MultispeQ results on Days 2 and 3 (Fig. S4C and 6C), suggesting that regulation of photosynthesis had partially acclimated.

Fig. S6G shows that the extent of dark-interval relaxation kinetics (DIRK) absorbance changes at 810 nm, showing that P_{700} became more oxidized when plants were exposed to chilling temperature (Fig. S6G, p<0.05). The rate constant for $P_{700}+$ re-reduction, as measured by the 810nm decay kinetics (k_{b6f}, Fig. S 6H, p <0.05), decreased at low temperature, implying that slowing of electron flow to PSI contributed to the observed net oxidation of $P_{700}+$. This effect likely reflects the onset of "photosynthetic control" (PCON) due to acidification of the thylakoid lumen and subsequent slowing of PQH_2 oxidation at the cytochrome *b$_6$f* complex (Chow & Hope 2004; Takizawa *et al.* 2008).

Fig. S6D shows the effects of temperature on the distribution of light-induced thylakoid *pmf*, as estimated by the ECSt parameter (Baker *et al.* 2007), normalized to relative chlorophyll content as described in

Materials and Methods. Low temperature-induced significant increases in the average ECSt (p<0.05), suggesting an increase in light-driven thylakoid *pmf*.

The proton conductivity of the thylakoid (*g*H+, Fig S6E), which predominantly reflects the activity of the thylakoid ATP synthase was significantly decreased at LT compared to CT (p <0.05), likely indicating a temperature-dependent decrease in the chloroplast ATP synthase activity. Fig. S6F shows that the average *v*H+, an estimate of the light-driven proton flux through both LEF and CEF (Takizawa *et al.* 2008), decreased at low compared to control temperature (p <0.05), similar to changes in LEF and Φ_{II}. The ratio of *v*H+/LEF, an indicator of the extent of cyclic electron flow (CEF) (Avenson, Cruz, Kanazawa & Kramer 2005a; Baker *et al.* 2007), was higher under LT compared to CT (Fig S6K).

Overall, these results indicate substantial alterations in control or regulation of photosynthetic processes on the third day of CT exposure, with (on average) and increase in CEF and decreases in ATP synthase activity, leading to increased *pmf* and PCON, and substantial increases in NPQ and decreases in Φ_{II} and LEF. However, there were strong variations in these responses, likely reflecting genetic differences across the population.

Detailed QTL results for MultispeQ parameters are shown in Figures S7-8 and Table S5. Several QTL intervals were identified in photosynthetic parameters in both CT and LT (Chrs 4, 6, 8 and 9 etc); we focus here on intervals on Chrs 4, 8 and 9, which showed potential overlaps with those found using the DEPI platform (Figs. 3 and 4). Figure 6 shows associations for selected QTL intervals on Chrs 4, 8 and 9 in the form of "Daisy Graphs," in which specific QTL intervals are indicated in the center circles, different phenotypes are indicated by surrounding circles, with the thickness of the connecting lines set proportional to the LOD score for association. The solid lines represent significant positive associations between the phenotype and the allele present in the tolerant (CB27, orange) and sensitive (24-125B-1, blue) lines. The overlap in these regions is consistent with co-association of the phenotypes to genetic loci in these regions, though as discussed below, we cannot rule out the participation of multiple loci.

Daisy plots for QTLs showed linkages to QTLs regions on Chrs 4 (marker positions 59.04-64.45 cM), 9 (marker positions 86.93-104.15 cM) under both CT (Panels A and B) and LT (Panels D and E), similar to the results from DEPI. The Chr 4 interval showed negative associations with the CB27 alleles for one set of parameters (Φ_{II}, k_{b6f}, vH+, gH+, ECSt, and qL) but positive associations for P700+. (Such a positive association means that the presence of the CB27 allele tends to increase the value of that parameter). Only weak associations were observed for relative chlorophyll content (SPAD) and NPQt. Strikingly, the Chr 9 region showed the inverse relationships, i.e. positive associations with the CB27 alleles for one set of parameters (Φ_{II}, k_{b6f}, vH+, gH+, ECSt, and qL) and negative associations for P700+. These results suggest that the loci on Chrs 4 and 9 have opposing effects on photosynthetic responses (see below).

A comparison of CT and LT (Figs. 4 D and E) shows that the patterns of associations to QTLs on Chrs 4 and 9 were similar, except that significant associations with NPQt only appeared under LT, most obviously to the region on Chr 9. These results are consistent with those from DEPI and suggest that, while the regions on Chrs 4 and 9 had qualitatively similar effects on most photosynthetic parameters, these were linked to increased photodamage or photoinhibition, specifically under low temperature.

A distinct pattern of associations appeared for the region on Chr 8 (Panels E and F, marker positions 22.81- 28.59 cM), which showed no significant associations under control temperature, but significant associations with Φ_{II} and NPQt under low temperature. The lack of connections to the other photosynthetic parameters suggests that Chr 8 controls NPQt through a mechanism that is distinct from that controlled by Chrs 4 and 9 (see also below).
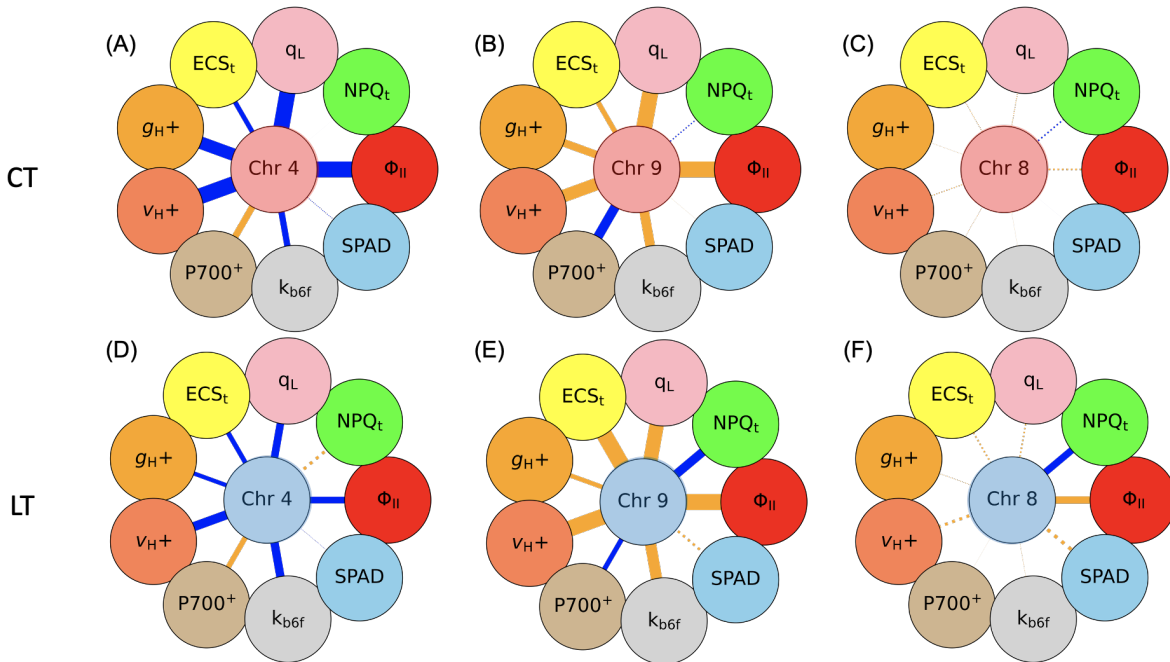

Figure 6. The associations for selected QTL intervals of photosynthetic parameters from MultispeQ in CT (A-C) and LT (D-F) at Chr 4, 59.04-64.45 cM (A and D) and Chr 9, 86.93-104.15 cM (B and E), Chr 8, 22.81- 28.59 cM (C and F). LOD score plots from previous figures (S7 and 8) were replotted as in the form of "Daisy Graphs," in which specific Chr is indicated in the center circles, different phenotypes are indicated by surrounding circles, with the thickness of the connecting lines set proportional to the LOD score for association (Max LOD 10 is set to 10, so above the LOD 10 is shown as same max thickness). (For details of each plot, refer to original figures, S7 and S8). Solid lines represent significant positive associations between the phenotype and the allele present in the tolerant (CB27, orange) and sensitive (24-125B-1, blue) lines. Below the threshold, each phenotype is shown as dashed lines.

Effect size contributions of specific QTL intervals to photosynthetic phenotypes.

In this section, we explore the effect sizes and directionalities of genetic markers on the observed phenotypes. Individuals of the RIL population are homozygous for each marker in the two parental lines, as indicated by the designations of either AA, having the allele from CB27 (tolerant, maternal line), or BB, having the allele from 24-125B-1 (sensitive, paternal line).

We first estimated genetic contributions from the QTL on Chrs 4 and 9 individually, by dividing the population into groups, having AA or BB markers at the peak positions for the two QTLs. The examples in Figs. 7 A-D show the effects of QTL intervals on Chrs 4 and 9 on Φ_{II} (04-2,3-Φ_{II}-CT/LT and 09-2-Φ_{II}-CT/LT) and qlt (04-2,3-qlt-LT and 09-2-qlt-LT) at 1.5 hr prior to the end of day 3. This time point was chosen because it reflects both immediate changes in photosynthesis and the accumulation of photodamage or photoinhibition. However, as implied by the timeline in Fig. 4, similar results will likely be observed over a range of time points.

At CT, genotypes with the AA allele at 04-2,3-Φ_{II}-CT showed a lower average Φ_{II} compared to those with the BB allele (Fig. 7A). The opposite effect was seen for the QTL on Chr 9, where the AA allele conferred a higher Φ_{II} compared to BB. At CT, no difference was seen in qlt between the parent lines, indicating that the effects on Φ_{II} and other processes did not result in the accumulation of substantial amounts of photoinhibition (Fig. 7B).
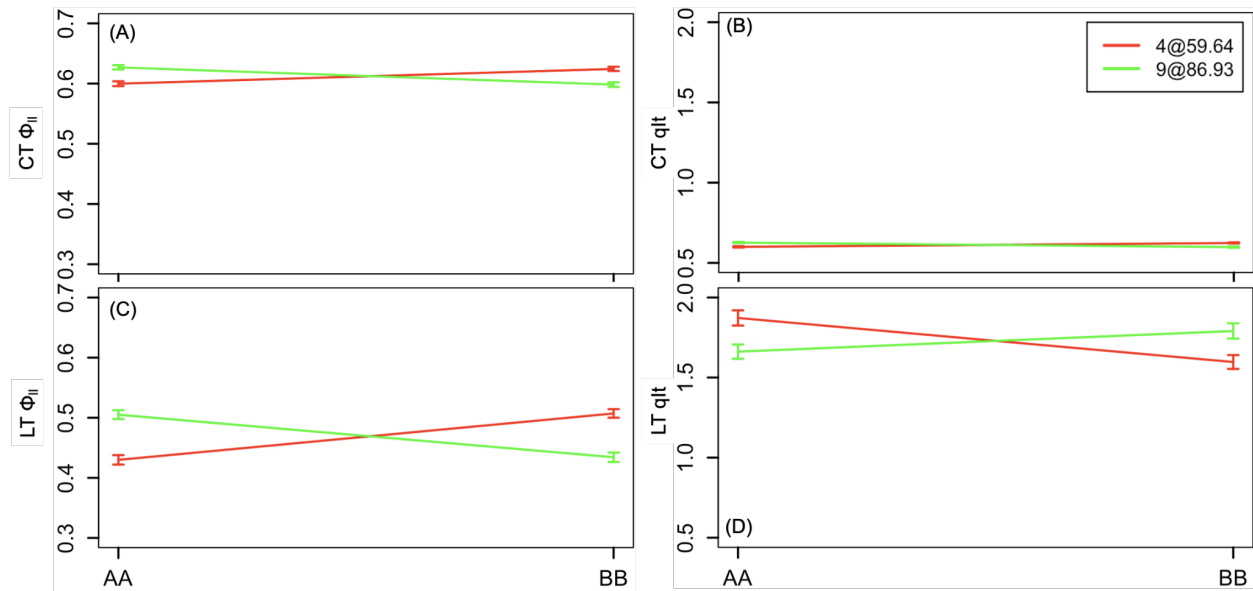
Across all genotypes, going from CT to LT resulted in decreased in Φ_{II} and increased in qlt. However, qualitatively similar trends were seen for the dependence on alleles at Chr 4 and 9 for Φ_{II} (04-2,3-Φ_{II}-CT/LT and 09-2-Φ_{II}-LT) and qlt (04-2,3-qlt-LT and 09-2-qlt-LT), but with substantially larger effect sizes in LT.

Larger genotypic effects were observed for qlt. Plants with the AA allele at Chr 4 showed higher average qlt values compared to those with BB, while plants with the AA allele at Chr 9 showed lower average qlt values compared to those with AA (Fig. 7B). This result is consistent with stronger LT-induced effects that result in the accumulation of photodamage.

To test for additivity or epistasis, we assessed the combined effects of both sets of alleles (Figs. 7 E and F), dividing the population into the four possible genetic combinations, AAAA, AABB, BBAA and BBBB for alleles from each parent for Chr 4 and Chr, e.g. the AABB genotype has the CB27 allele on the Chr 4 QTL and that for 24-125B-1 in the QTL on Chr 9. Note that AAAA and BBBB showed no significant differences under both conditions and parameters (Fig. S9), and thus we present averaged AAAA and

BBBB for each parameter and condition, only showing three groups in Fig 7 E-F. Under both temperatures, the AABB genotypes showed the lowest Φ_{II}, while the BBAA genotypes showed the opposite extreme. The AAAA and BBBB genotypes showed only small differences, suggesting that the effects of the two alleles canceled each other out in these genotypes. These results suggest that polymorphisms within the QTL on Chrs 4 and 9 have additive, but opposite effects on Φ_{II}, under both temperatures. These trends were more extreme under LT, suggesting that the lower temperature accentuated the genotypic effects.

Interestingly, qualitatively different effects were observed for qlt between CT and LT. At CT, only small effects were seen between the AABB and BBAA genotypes, suggesting that the differences in Φ_{II} or other properties did not impose large differences in photodamage or photoinhibition. By contrast, large genetically-controlled effects were seen at LT, with the AABB genotypes showing the largest extents and BBAA showing the smallest. These results support the model where interactions between temperature and genotypes were sufficiently severe that they led to substantial differences in photodamage.
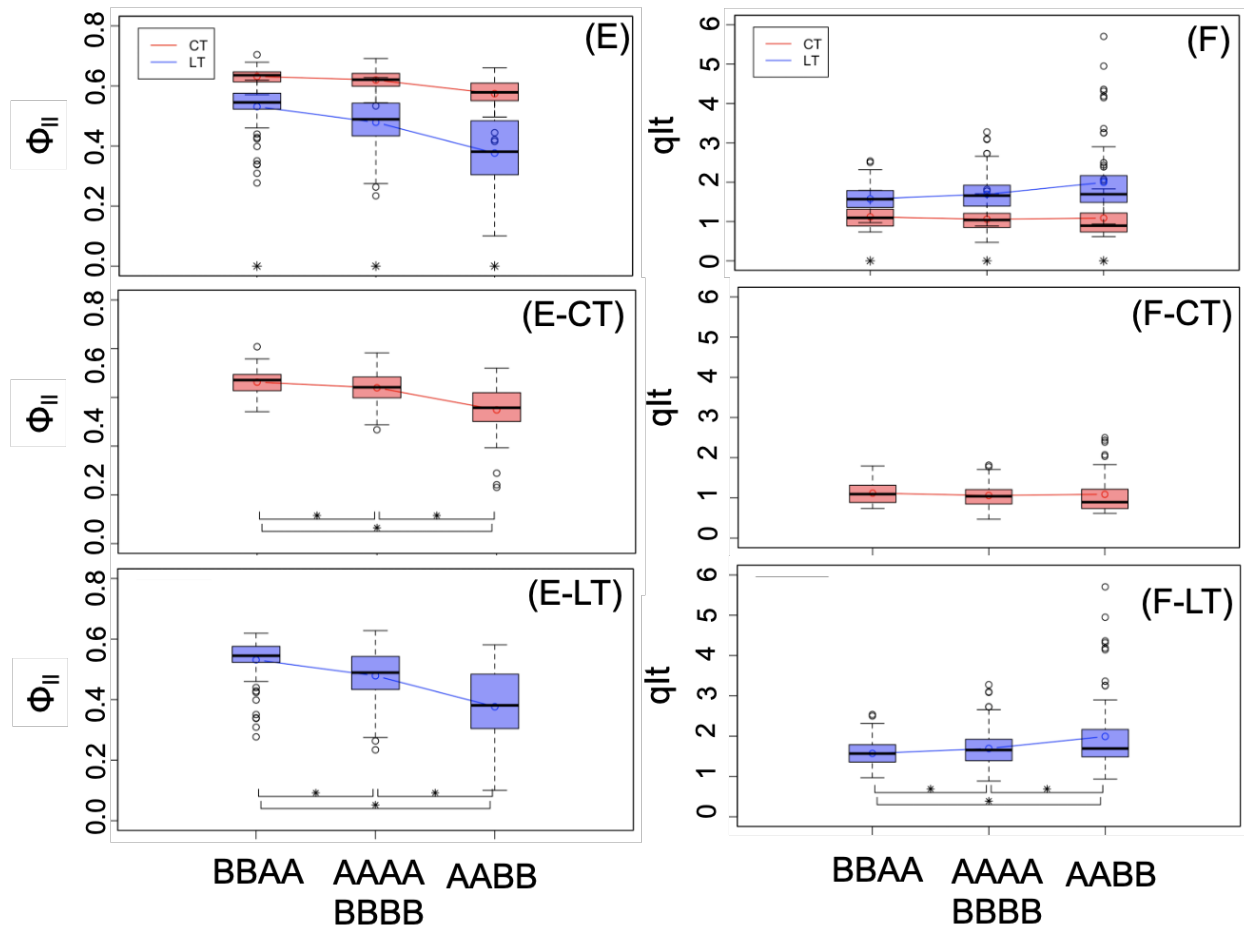
Figure 7. Effect plots (A-D) and box plots (E-F) of identified QTLs in Chrs 4 and 9 for Φ_{II} and qlt at 1.5 hr prior to the end of Day 3 (206 µmol, m^{-2}, s^{-1}). (A-D) Each panel shows the mean of Φ_{II} (A,C) and qlt (B,D) by indicated as y-axis in each condition (CT: A-B and LT: C-D) against allele (either AA or BB) at identified QTLs in chr 4, 59.64 cM (red) and 9, 86.93 cM (green). (E-F) Box plots for Φ_{II} (E) and qlt (F) in both conditions (CT and LT are colored by red and blue respectively) grouped by alleles from identified QTLs in Chrs 4 and 9, AABB, BBAA and averaged AAAA and BBBB. The line connects each mean of the group. Significant differences between conditions for each group (p<0.05, t-test) are shown as the asterisk at the bottom of the plots. (E-CT/LT, F-CT/LT) Significant differences of Φ_{II} or qlt between groups (p<0.05, t-test) are shown as the asterisk in the bottom of the plots for each condition.

Genetic effects on photoinhibition at low temperature are predominantly controlled by altering rates of photodamage.

The results above suggest that the major QTL polymorphisms impact photosynthesis under both CT and LT, but have cumulative, substantial secondary effects on PSII photoinhibition, as estimated by chlorophyll fluorescence, only at the lower temperatures. Two basic mechanisms have been proposed to control the extent of PSII photoinhibition, altering the rates of PSII photodamage, and altering the rates of

22

PSII repair (Aro *et al.* 1993; Murata, Takahashi, Nishiyama & Allakhverdiev 2007). To distinguish between these mechanisms, we measured (Fig. 8) the effects of illumination with high light (1000 µmol m^{-2}, s^{-1}) on maximal PSII quantum efficiency (Fv/Fm) in the presence and absence of lincomycin, which blocks PSII repair by inhibiting protein synthesis in the plastid (Tyystjärvi & Aro 1996). Because the effects of the alleles in the QTLs for Chrs 4 and 9 partly compensated for each other, we compared the two parental lines (CB27 and 24-125B-1, Fig. 8A and B) and two selected progeny lines (Fig. 8C and D) that contained the AABB and combinations of alleles for the QTL on Chr 4 and 9 and showed the largest differences in Φ_{II} values (Fig. 8F): RIL-60, with genotype BBAA, which at LT showed the highest Φ_{II} and lowest qIt values at LT, while RIL-4, with genotype AABB, showed the smallest Φ_{II} and largest qIt values.

In the absence of lincomycin, the parent lines show only small differences in loss of PSII efficiency during exposure to high light (Fig. 8A). However, when infiltrated with lincomycin, the sensitive (24-125B-1) showed stronger losses of PSII efficiency that proportionally increased at lower temperatures (Fig. 8B). These results imply that PSII was photodamaged more rapidly in the sensitive line, but that repair was sufficient to maintain similar steady-state levels of PSII activity in the two lines. Stronger effects were observed between RIL-4 and RIL-60, which showed progressively larger increases in photoinhibition, even in the absence of lincomycin. These effects were larger in the presence of lincomycin, suggesting that a substantial fraction of the increased photoinhibition was caused by increased rates of photodamage, with smaller contributions from repair.
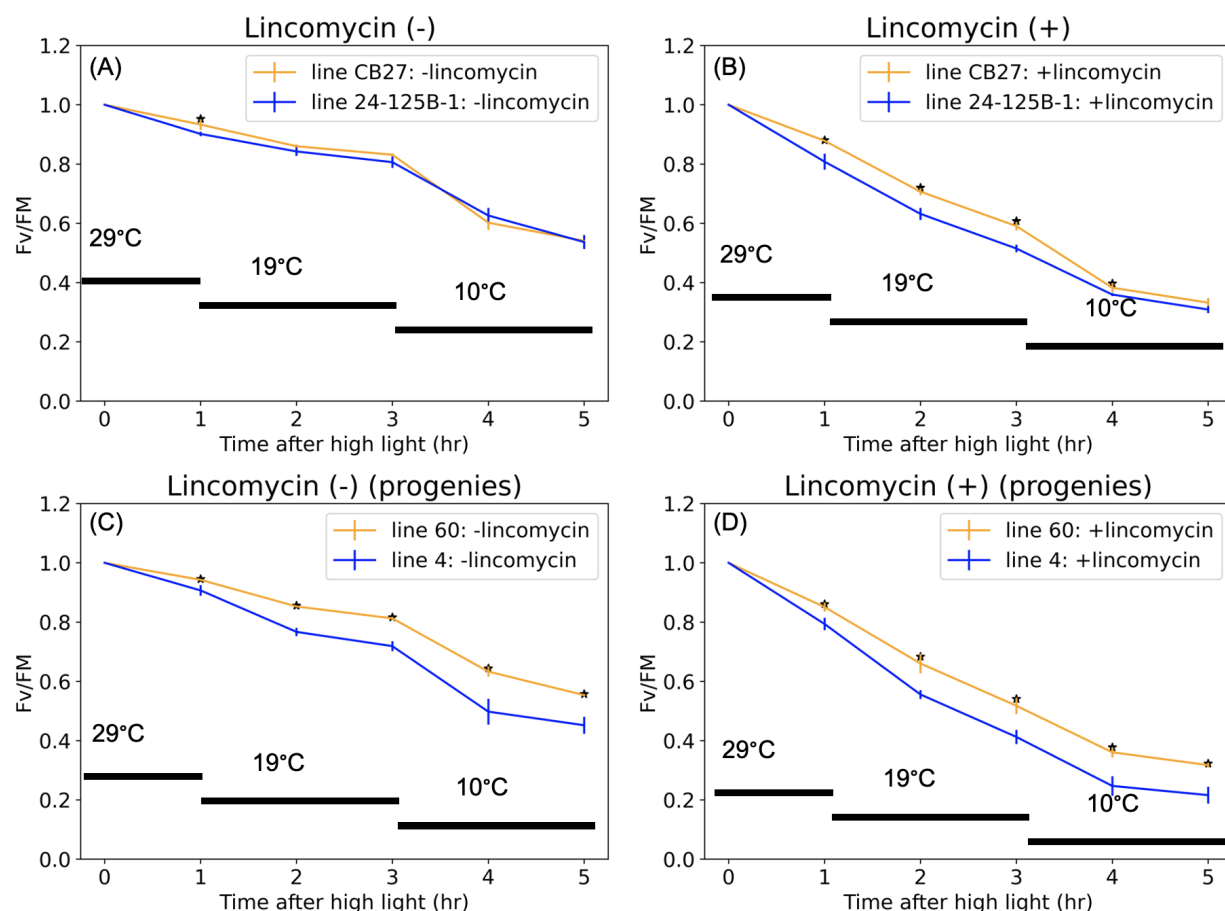
Figure 8. PSII photodamage and repair during exposure to high light at a range of temperatures.
Relative changes in the quantum efficiency of photosystem II (PSII) estimated by the saturation flash-induced increases in chlorophyll fluorescence, measured in darkness as described in Materials and Methods. Two pairs of genotypes were compared: Panels A and B show comparisons between the two parental lines and Panels C and D compare two selected progeny lines that contained combinations of alleles for the QTL on Chr 4 and 9 that consistently showed the largest (RIL-60, with genotype BBAA) and lowest (RIL-4, with genotype BBAA) effects on Φ_{II} in the experiments described in Fig. 5. Intact, detached unifoliate leaves, comparable to those imaged during the experiment described in Fig. 1, were vacuum infiltrated with either 0.2 g/L lincomycin (B and D) to prevent PSII repair, or deionized water as a control (A and C) and floated on these solutions during exposure to high light to prevent drying. Measurements were conducted using the DEPI chamber described in Figure 1, but leaves were exposed to constant, high light (1000 µmol, m^{-2}, s^{-1}) for one hour under a sequence of decreasing temperatures, from control or growth temperature (CT, 29°C), low temperature (LT, 19°C, as used in the DEPI experiments shown in Figures 1) and very low temperature (10°C). Values of F_v/F_M'' were measured periodically during the experiment, after a 20 minutes dark period to allow for relaxation of qE, and normalized to the maximum PSII efficiency measured in dark-adapted samples (F_v/F_M). The averaged replicates (n≥3) ± S.D are shown.

The photosynthetic proton circuit and Q_A redox state modulate the genetic effects on temperature stress

To explore possible mechanisms for the increased rates of photodamage in the sensitive lines, we assessed the genotype dependencies of more detailed photosynthetic parameters taken with MultispeQ across the entire RIL population, as in Fig. S6. Figure 9A shows average values of qL against Φ_{II} at the peak light intensity at CT and LT (Day 3), grouped by their genotypes for QTL on Chr 4 and 9, i.e., those with AAAA, AABB, BBAA and BBBB, as in Fig. 7.

For CT, there was a continuous, nearly linear relationship between qL on Φ_{II}. However, genotypes having the BBAA and AABB genotypes showed the highest and lowest values for both parameters ($p<0.05$ by t-test), while those with AAAA and BBBB showed intermediate values (NS) (Fig. S10).

A qualitatively similar trend was observed at LT, but with markedly stronger decreases in the AABB compared to the BBAA genotypes, with qL reaching substantially lower values. These results are consistent with models where increased PSII excitation pressure (Huner, Öquist & Sarhan 1998), caused by the accumulation of reduced Q_A, caused increased rates of PSII photodamage at LT, with this effect being stronger in the genotypes containing the AABB alleles.

Fig. 9 B shows the dependence of NPQt on ECSt, measured using the MultispeQ as in Fig. S6. It was not possible to distinguish between qE and qI using the rapid MultispeQ protocol, but the observed positive dependence of NPQt on *pmf* is consistent with qE being the major form of NPQt in CT. The genotypic subgroups showed different distributions along with this overall trend, with the tolerant RILs (BBAA) tending to have the highest values for both NPQt and ECSt, while the sensitive RILs (AABB) showed the opposite, i.e. tending towards the lowest values for both NPQt and ECSt, and the intermediate RILs (AAAA and BBBB) largely showed intermediate values for both parameters. These distributions suggest that, at CT, the QTLs of Chr 4 and 9 contribute to the qE response through effects on the extents of thylakoid *pmf*, with the AABB genotypes tending to have lower ECSt and correspondingly lower NPQt.

A strikingly different behavior was seen at LT, where a negative correlation was observed between NPQt and ECSt, i.e., higher NPQt was associated with lower, rather than higher, *pmf*. This result is the opposite of what one would expect if the major form of NPQt contributed by qE, but instead supports a model where photoinhibition (qIt) is the dominant form of NPQt. Under these conditions, the AABB genotypes showed the lowest ECSt and the largest NPQt, with many genotypes reaching quite large NPQt extents. This result supports the conclusions drawn from the DEPI results (Figs. 1 and S6) which show a shifting of contributions to NPQt from qEt to qIt at LT. These results are consistent with a breakdown in the

relationship between *pmf* formation and activation of qEt at LT that is modulated by the alleles in QTL on Chr 4 and 9.

Figure 9C compares ECSt with the thylakoid proton conductivity, *g*H+, which is largely controlled by the activity of the ATP synthase (Kanazawa & Kramer 2002). Overall average *g*H+ values were lower at LT compared to CT, but remained similar across the genotypic groups at each temperature. The apparent lack of genetic contributions to *g*H+ appears to argue against a role for modulating ATP synthase activity in LT responses.
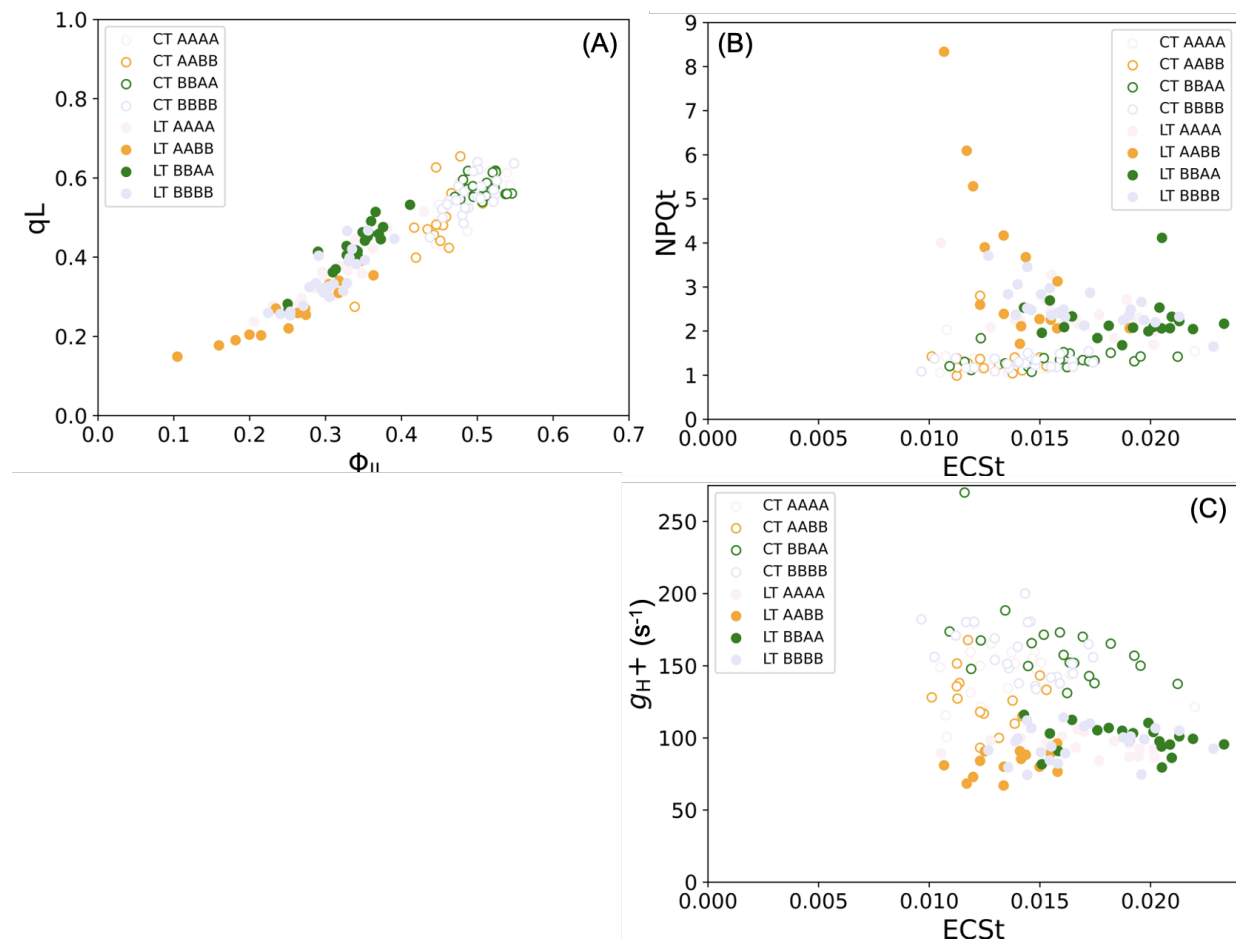

Figure 9. Relationships between photosynthetic responses grouped by different combinations of alleles for the identified QTLs in Chrs 4 and 9 for both conditions, CT and LT (CT: opened, LT: closed symbols). (A) qL against Φ_{II} from DEPI data, middle of day 3 (highest light intensity, 500 µmol photons m^{-2} s^{-1}). NPQt against ECSt (B) *g*H+ against ECSt (C) from MultispeQ data, middle of day 4 (highest light intensity, 500 µmol photons m^{-2} s^{-1}). The allele groups of AAAA, BBBB are indicated by light pink and light purple, respectively. The allele groups of AABB and BBAA are colored orange and green, respectively. Detailed Statistical analyses testing for differences in phenotypes between the allele groups are shown in Fig. S10.

Nyctinastic leaf movements (NLM)

During analyses of the DEPI video, we observed large variations in nyctinastic leaf movements (NLM) among RILs population. NLM are motions of leaves. Typically circadian-regulated, induced by changes in the volume of motor cells in the pulvinus, an organ at the base of the petiole (Herbert 1992). NLM appeared specifically under LT conditions on Day 3, suggesting a connection with temperature responses. Indeed, earlier work proposed that low temperature-induced photoinhibition can be partially alleviated by such leaf movements (Huang, Zhang & Cao 2012; Huang, Zhang, Zhang & Hu 2014). Thus, we aimed to determine if variations in NLM could be related to other effects of LT on photosynthesis, and if these effects are related to those controlled by the major QTL intervals on Chrs 4 and 9.

The differences in NLM during LT are readily seen in the example images in Fig. 10 (A) (see also Fig. S - Video 1) in which parent line CB27 showed strong paraheliotropism (leaves pointing up) in the early morning but fully opening within 4 hours of light. By contrast, 24-125B-1 remained nearly fully open (diaheliotropic) under all conditions. As described in Fig. S-NLM (A) (see also Materials and Methods), we devised a method for estimating the relative extents of NLM over time. As shown in Fig. S-NLM (B), we observed a wide range of NLM phenotypes in the RIL population, with some genotypes showing extents of motions that exceeded those seen in the two parents (see Fig. S-Video 1).

Fig. S-NLM (C-D) shows a time-resolved heat map for NLM LOD scores. The strongest associations appeared on Chrs 8, 10 and 11. The intervals were strongest within about 2 hours after start of illumination in the morning, when leaves were most rapidly transitioning from paraheliotropic to diaheliotropic positions. Additional leaf movement-related QTL intervals were seen (e.g., on Chrs 7 and 9 in the afternoon of Day 3), but appeared to be associated with nutation motions, related to differences in growth of the stems, and thus were not explored in detail. It is interesting to note, however, that these intervals did not overlap with those attributable to NLM, suggesting that different genetic components control these motions.

In principle, NLM can have both immediate effects, e.g. by affecting the instantaneous light absorption, and (potentially) longer-term effects, e.g. on the accumulation of photoinhibition. We thus compared LOD scores for associations across different time points.

Figure 10 (B) compares LOD scores for NLM, taken at 2 hours of illumination on Day 3 (at 301 µmol, m^{-2}, s^{-1}), where the associations were the strongest, with Φ_{II}, NPQt and qIt taken at 11.5 hours of illumination, when their associations were strongest (Fig. 2) but those for NLM associations had disappeared (Fig.S-NLM D). No significant overlap in QTLs was observed.
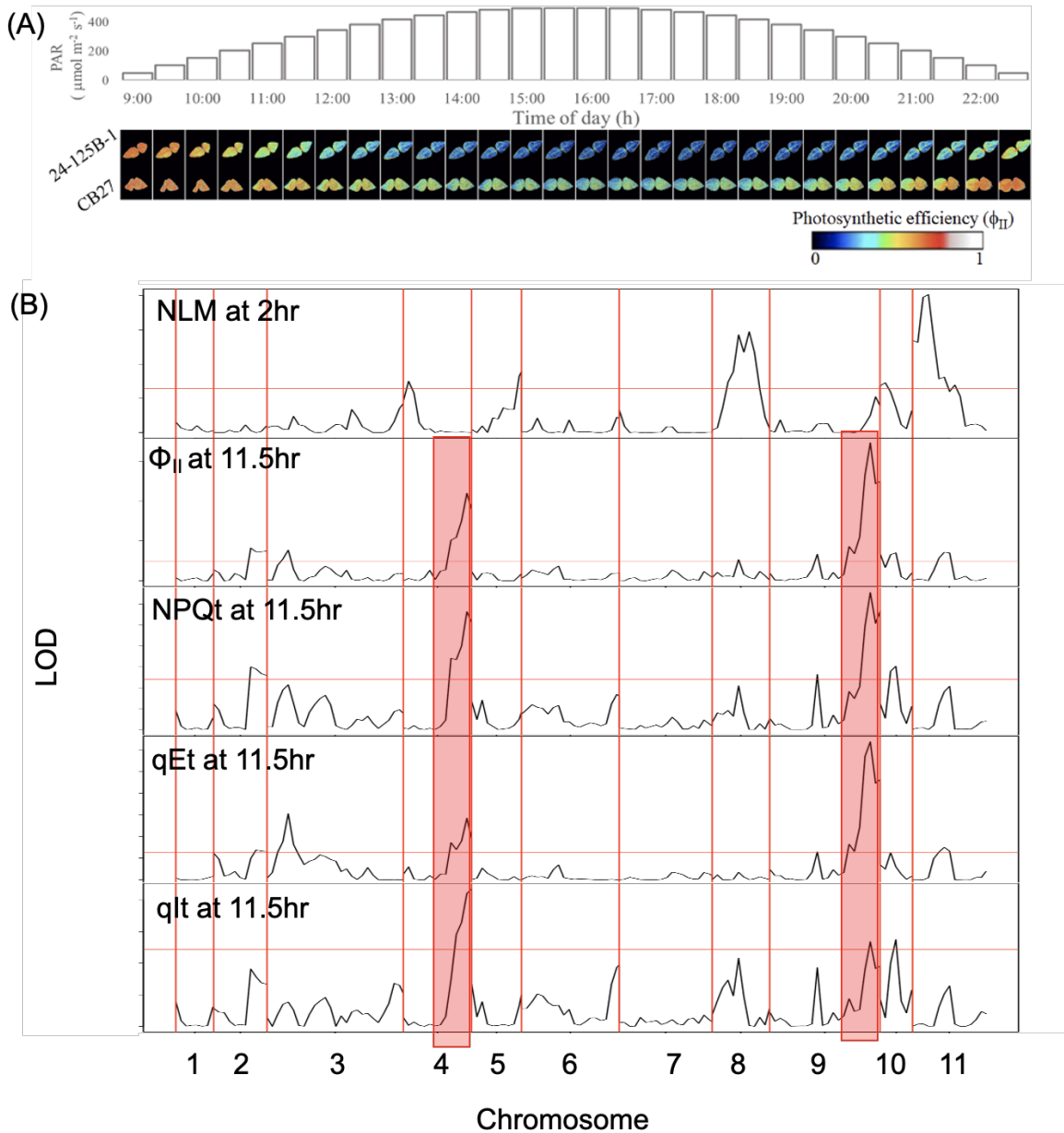
Figure 10. (A) Filmstrip view of sequential DEPI images showing changes in nyctinastic leaf movement (NLM) with false-coloring reflecting of ϕ_{II} values over the course of the day for the two parents during Day 2 of LT stress. The light intensity in the DEPI chamber was increased by ~ 50 μmol m^{-2} s^{-1} every 30 min and images were captured at the same interval at the end of every light intensity change over a 14-hour day. The top panel indicates the light intensity for each corresponding image. For the full dataset, see video in S-Video 1. **(B) Logarithm of odds (LOD) scores for QTL associations for nyctinastic leaf movements (NLM), ϕ_{II}, NPQt and qlt**. The timepoints for NLM at 2 hr after illumination (301μmol, m^{-2}, s^{-1}) and ϕ_{II}, NPQt and qlt at end of Day 3 at 11.5 hr after illumination (301 μmol, m^{-2}, s^{-1}) on Day 3 LT conditions. The red dotted horizontal line represents the LOD threshold determined by permutation test at $p<0.05$.

However, some overlap was observed between photosynthetic and NLM intervals at the end of Day 3 at 14 hr after illumination (51 µmol, m^{-2}, s^{-1}) (Fig. S-NLM (E) Chr 8 and Φ_{II}, NPQt and qIt, indicating possible linkages between NLM and photoinhibition. However, no overlaps were observed between the QTL intervals for NLM and those for the photosynthetic phenotypes on Chrs 4 and 9, where the genetic loci we found genetically controlling photoinhibition under LT. This result suggests that effects of variations in NLM on photosynthetic properties were likely to be independent of those controlled by Chrs 4 and 9.

Fig. S-NLM (F-M) quantifies the effect on NLM at times between 0.4 and 2 hours after illumination of alleles (either AA or BB) at identified QTLs in chr 8, 28.59 cM (red) (A and B). The allele of AA group imposed lower NLM, indicating more paraheliotropic positions, while the BB group imposed more diaheliotropic positions. We additionally compared the allele group of Chr 4 (F-I, green) and Chr 9 (J-M, green) to confirm QTL results, that the alleles under the QTL on Chrs 4 and 9 did not impose significant differences in NLM.

Mechanistic interpretations of the QTL associations.

A range of different processes could result in decreased photosynthetic capacity and photodamage observed at LT. The questions we address in the current work are: which of these processes is modulated by the genetic diversity in the RIL population? How are these effects linked mechanistically? Which of these may contribute to the relative sensitivities of the plant to chilling stress?

The light reactions are known to be controlled by a range of processes that can be (roughly) categorized in the following (see reviews in (Avenson *et al.* 2005b; Cruz *et al.* 2005)): 1) Limitations in forward reactions, e.g. slowing of electron or proton transfer, leading to buildup of intermediates. In our work, we probed several indicators of these processes, including the redox state of Q_A through the qL parameter, the redox state of P700 and PSI acceptor side electron carriers, the buildup of the thylakoid *pmf*, and the control of electron flow by the cytochrome b6f complex (PCON). 2) Dissipation of captured energy. In vascular plants, this occurs most notably through NPQ, either by rapidly inducible and reversible qE or slower processes, including photoinhibition of PSII (qI) and the accumulation of zeaxanthin (qZ). Both categories of processes are influenced by both the capture and utilization of light energy, the energetic matching of these controls the buildup of energetic intermediates of the light reactions. Efficient and safe matching required the chloroplast to balance not only the amount of energy input and used, but the fractionation of this stored energy into NADPH and ATP.

Using the rapid, high throughput methods employed here, we were able to test for the involvement of the following important processes (See Fig. 11):

A. PSI acceptor-side limitations can occur when electrons accumulate on PSI electron acceptors (NADPH, ferredoxin, F_A, F_B) preventing further LEF.

B. PSII acceptor limitations occur when electrons accumulate on Q_A (decreased qL), blocking PSII photochemistry.

C. Energy-dependent NPQ (q_E) and photosynthetic control activated by acidification of the thylakoid lumen. Metabolic or physiological limitations can result in decreased ATP synthase activity, causing a build-up of pmf. The pH component (ΔpH) of pmf acidifies the lumen, controlling electron transfer through the cytochrome b_6f complex, and induces violaxanthin de-epoxidase, leading to the conversion of violaxanthin (V) to antheraxanthin and Zeaxanthin (Z) and the protonation of PsbS, resulting in quenching of excitation energy through the q_E mechanism.

D. Photoinhibition. In the light, PSII centers can be damaged, directly decreasing the number of active PSII centers, while initiating long-lived photoinhibition-related NPQ (q_I). Subsequent repair processes restore active PSII centers. The temperature could be affected by the rate of photodamage and repair.

E. Photosynthetic control (PCON) is the control of electron flow related to the acidification of the thylakoid lumen and subsequent slowing of PQH_2 oxidation at the cytochrome b_6f complex (Chow & Hope 2004; Takizawa *et al.* 2008).

F. Cyclic electron flow (CEF) involves transfer of electrons from the acceptor side of PSI back to the plastoquinone pool, generating ATP without net reduction of NADPH (). CEF can thus augment the production of ATP to balance the ratio of ATP/NADPH to meet downstream metabolic needs (Kramer, Avenson & Edwards 2004). The plastoquinone reductases are regulated by ATP levels, allowing for very rapid balancing of ATP/NADPH production (Fisher, Bricker & Kramer 2019). CEF can also result in acidification of the thylakoid, and thus contribute to PCON and the induction of qE.

G. Regulation of the chloroplast ATP synthase. The ATP synthase controls the rate of proton efflux from the lumen. The activity of the ATP synthase is regulated or controlled by a number of factors, including the redox state of the thiol groups on the gamma subunit and the availability of substrates ADP and Pi, which are, in turn, impacted metabolic or physiological state of the chloroplast, resulting in differential accumulation of *pmf* and acidification of the lumen, affecting PCON and qE.

H. Nyctinastic leaf movements (NLM) can adjust the amount of light absorbed by a leaf by changing leaf angle with respect to that of solar influx (Herbert 1992).

The analysis of the RIL library under CT and LT conditions revealed genetically controlled variations in many of these processes. Two notable exceptions were ATP synthase activity (*g*H+, Figs. 5E, 9C) and PSI overreduction (Y_{NA}). We did observe a general reduction on *g*H+ going from CT to LT (Fig. S6E), as one would expect if the capacities for electron and proton flow and assimilation (Kanazawa & Kramer 2002), sink strength (Takizawa *et al.* 2008) or onset of limitations at triose-phosphate utilization (Yang, Preiser, Li, Weise & Sharkey 2016) were decreased at the lower temperature (Allen & Ort 2001; ORT 2002). However, the effect was not significantly different in the two parent lines, nor we did not observe strong linkages to genetic markers, suggesting that modulation of ATP synthase activity did not contribute to the differences in chilling sensitivities, under the RIL population and under our conditions. These

results suggest that, in our RIL population, photosynthesis is tuned to prevent these limitations. It is possible, though, that a different population could exhibit such variations and these may affect chilling tolerance.

The lack of effects on Y_{NA} are interesting in light of the proposal that PSI photodamage, related to over-reduction, is a major factor in chilling-induced photodamage damage in some species, notably *Cucumis sativus* (Sonoike 1996), and in mutants that lack the ability to activate PCON (Tikkanen *et al.* 2012; Takagi, Takumi, Hashiguchi, Sejima & Miyake 2016; Kanazawa *et al.* 2017). Despite being quite chilling sensitive, we did not see any evidence for PSI over-reduction in cowpea. Instead, we observed strong PCON (Fig. S6H) which resulted in net oxidation of P700 (Fig. S6G), preventing the accumulation of electrons on PSI electron acceptors. Consistent with this result, we found no significant differences in the loss of active PSI at LT, as measured by the extent of maximal light-induced absorbance changes at 810 nm, between the two parent lines after either LT or CT exposure ($p>0.7$).

We also observed strong induction of NLM specifically under LT (Fig.S-NLM C-D). It has been proposed that these may protect against chilling damage to photosynthesis in some species (Huang *et al.* 2012, 2014). However, we did not observe obvious linkages to processes we measured, including long-term changes in NPQt (Fig. 10B), arguing against strong impact, at least under our conditions.

The apparent colinkages of photosynthetic parameters to QTLs on Chrs 4 and 9, and the order of their appearance, suggests a model where the control of the light reactions by these loci is associated with increased thylakoid *pmf* (Figs. 5D and S6D), attributable to the activation of CEF (Figs. 5I and S6K), which results in increased qE, more reduced Q_A and oxidized P_{700}+. While these effects are seen under both experimental temperatures, they appear to have secondary effects at LT, resulting in strong differences in photoinhibition (Figs. 1, 4, 8 and S3, 4), mainly caused by increased rates of photodamage (Fig. 8). This results in a strong shift in the sensitive lines, from qE to qI as the major form of NPQ (Figs. 1 and S3, 4). This increased photodamage rate is associated with a net reduction of Q_A (Figs. 1E, 5C, 9A and S3E, S4E) and elevated *pmf* (Figs.5D and S6D), both of which will increase the rates of recombination reactions within PSII, resulting in the production of toxic singlet O_2 (Ivanov *et al.* 2012; Telfer 2014; Davis *et al.* 2016), and we thus propose this effect as the major contributor to the observed differences in chilling sensitivity of the light reactions. Such a mechanism is also consistent with the order of appearance of the linkages we observed in the time-resolved DEPI experiments, where qEt, qL and qIt preceded effects on Φ_{II} and NPQt (Figs. 3 and 4).

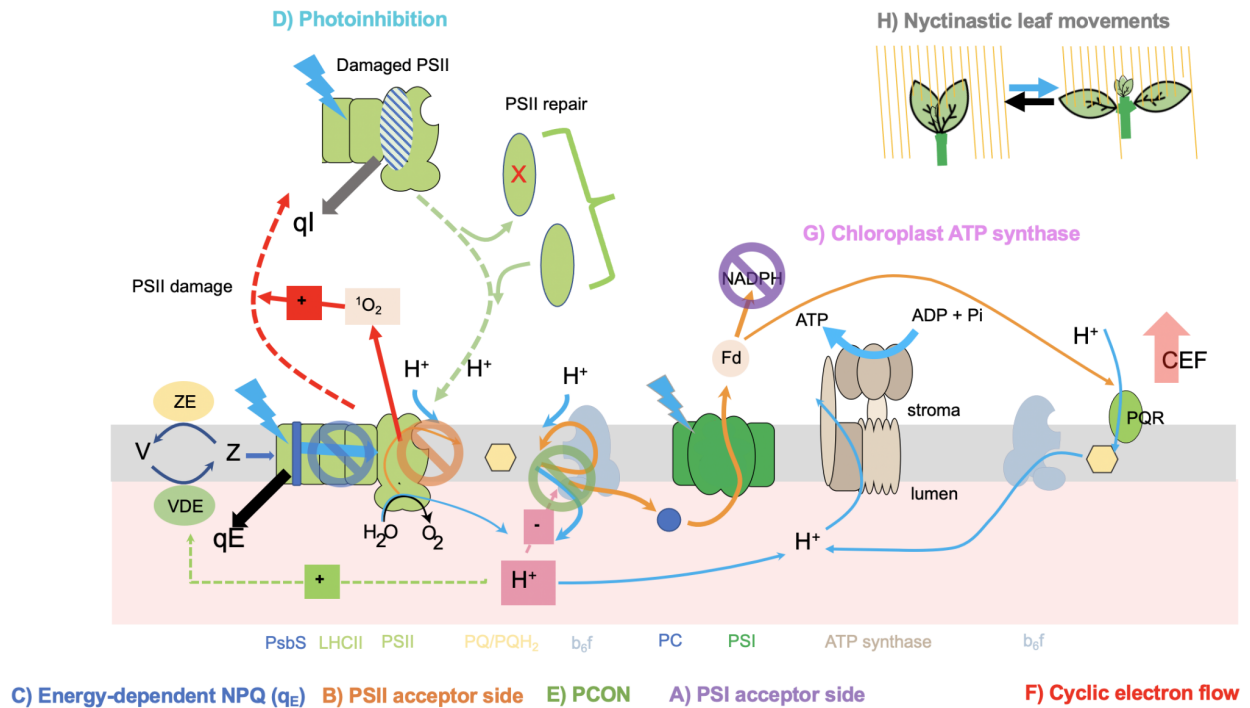**Possible mechanisms limitation to LEF at low temperature**

D) Photoinhibition

Damaged PSII

PSII repair

H) Nyctinastic leaf movements

qI

PSII damage

$^1O_2$

ZE

V   Z

VDE

qE

H_2O O_2

H^+ H^+

H^+

G) Chloroplast ATP synthase

NADPH

Fd

ATP   ADP + Pi

H^+

CEF

stroma

lumen

PQR

H^+

H^+

PsbS   LHCII   PSII   PQ/PQH$_2$ b$_6$f   PC   PSI   ATP synthase   b$_6$f

C) Energy-dependent NPQ (q$_E$)   B) PSII acceptor side   E) PCON   A) PSI acceptor side   F) Cyclic electron flow

Figure 11. Possible mechanisms limitation to linear electron flow (LEF) at low temperature (schematics for the regulation of light energy capture and storage by plant photosynthesis.) A) PSI acceptor-side limitations (purple), B) PSII acceptor limitations (orange), C) Energy-dependent NPQ (q$_E$) (blue), D) Photoinhibition (light blue), E) Photosynthetic control (PCON) (green), F) Cyclic electron flow (CEF) (red), G) Regulation of the chloroplast ATP synthase (pink), H) Nyctinastic leaf movements (grey).

Candidate genes in QTL intervals

We explored possible candidate genes in the minimum and maximum genetic range of QTL intervals in Chrs 4 and 9 that showed linkages for the photosynthetic parameters. First, based on the hypothesis that a common polymorphism will be responsible for the collective phenotypes associated with a QTL region, we determined which genes fell in the most likely intervals, encompassing the regions with LOD scores greater than the LOD significance threshold, common to all the phenotypes. Second, because we cannot exclude the possibility that multiple polymorphisms contribute to the observed phenotypes, we explored the broader range of genomic regions that encompassed the full textents of all associations from any photosynthetic phenotype with LOD scores above the threshold.

For the QTL interval on Chr 4, we considered 13 overlapping QTL intervals (04-3-Φ_{II}-LT, 04-3-NPQt-LT, 04-3-qEt-LT, 04-3-qIt-LT, 04-1-qL-LT from DEPI and 04-1-ECSt-LT, 04-1-gH+-LT, 04-1-LEF-LT, 04-1-P700+-LT, 04-1-Φ_{II}-LT, 04-1-qL-LT ,04-1-vH+-LT, 04-1-kb6f-LT from MultispeQ), from which predicted the most likely common region as between 60 - 60.93 cM (flanking markers, 2_00148 and 2_07328), and

contains 79 candidate genes (Table S6). One interesting candidate gene in this region is Deg1 (*Vigun04g188700*), a protease localized in the thylakoid lumen that is known to be involved in PSII repair, by degrading damaged D1 (Kapri-Pardes, Naveh & Adam 2007) and OE33 subunits of PSII, as well as PC (Chassin, Kapri-Pardes, Sinvany, Arad & Adam 2002). *deg1,* RNA interference transformed *Arabidopsis thaliana* with a reduced level of Deg1, is more sensitive to photoinhibition, showing accumulated D1 protein (inactive form) and less of its degradation products (Kapri-Pardes *et al.* 2007). A role for Deg1 in modulation of the PSII repair cycle is consistent with our results, showing associations among Chr 4 genotypes, Φ_{II} and qlt (Fig. 7C-D) at LT, suggesting that certain alleles within this region show lower photoinhibition likely related to increase PSII repair. The broader (more inclusive) region of the Chr 4 QTL region, which extended between 34.47 - 64.45cM (flanking markers, 2_10801 and 2_04962) encompassed a total of 712 predicted coding regions (Table S7). This region included several additional photosynthesis-related genes, including the light-harvesting complex of photosystem II (LHCII) 5 (*Vigun04g167600*) and ferredoxin thioredoxin reductase (FTR) (*Vigun04g181000*), all of which could in principle contribute to chilling responses.

On Chr 9, we observed 14 overlapping QTL intervals (09-2-Φ_{II}-LT, 09-2-NPQt-LT, 09-2-qEt-LT, 09-2-qlt-LT, 09-2-qL-LT from DEPI, 09-1-ECSt-LT, 09-1-gH+-LT, 09-1-kb6f-LT, 09-1-NPQt-LT, 09-1-P700+-LT, 09-1-qL-LT, 09-1-vH+-LT, 09-2-LEF-LT, 09-2-Φ_{II}-LT from MultispeQ). The minimal common region was found to span 93.76-95.95cM (flanking markers, 2_11917 and 2_22085), containing 68 candidate genes (Table S8). One interesting candidate gene in this region is thioredoxin-h1 (trx-h1) (*Vigun09g249200*). Trx contains cysteine residues that are redox-active and reversely transfer the reducing potentials from light reactions to thiol-regulated enzymes. Trxs have conserved structures (WCGPC) to interact with target enzymes but react with different sets of target enzymes (Schürmann & Jacquot 2000; Collin *et al.* 2003; Yoshida, Matsuoka, Hara, Konno & Hisabori 2014; Geigenberger, Thormählen, Daloso & Fernie 2017). More than 20 isoforms of trx were found and categorized into several classes, trx f, h, m, x, y and z in the chloroplast (Collin *et al.* 2003; Yoshida *et al.* 2014; Geigenberger *et al.* 2017). Trx-h is eukaryotic trx and its potential target proteins are Triosephosphate isomerase, ADP-glucose pyrophosphorylase (AGPase) (Marx, Wong & Buchanan 2003), peroxiredoxins (Rouhier *et al.* 2001; Marx *et al.* 2003; Maeda, Finnie & Svensson 2004) and non-specific lipid transfer protein (Maeda *et al.* 2004). Ortiz et al 2017 also identified trx gene (*Sb03g004670*) from a genome-wide association study (GWAS) of Sorghum with chlorophyll fluorescence and carbon assimilation measurements at LT (Ortiz et al. 2017). This region also contains genes for the large subunit of AGPase (APL2, *Vigun09g247600*), which is involved in starch biosynthesis and regulated by trx-h. A homologous gene in *Arabidopsis* (At1g27680) was previous shown by Kilian et al (2007) to be upregulated upon exposure to low temperature (4°C), suggesting a possibility that carbon assimilation could be an underlying mechanism inducing natural variations in photosynthesis at low temperature, and this might be mediated by trx. Interestingly, recent research showed that trx-h2 is essential for cold tolerance by upregulating cold-responsive (COR) genes in *Arabidopsis* (Park *et al.*

2021). We found trx-h1, but there is the possibility that different isoforms of trx affect chilling tolerance in different species.

The broadest range for the Chr 9 QTL spanned the region between 56.08-104.15cM (flanking markers, 2_01496 and 2_23951), and encompassed 1242 predicted coding regions (Table S9). This region contained several photosynthesis-related genes such as Mog1/PsbP/DUF1795-like photosystem II reaction center PsbP family protein (*Vigun09g156000 and Vigun09g204000*), subunit NDH-M of NAD(P)H:plastoquinone dehydrogenase complex (*Vigun09g160700*), ATP synthase epsilon chain *(Vigun09g163500)*, photosystem II 22kDa protein (psbS) (*Vigun09g165900*), ferredoxin-related (*Vigun09g220600*), photosystem II subunit X (*Vigun09g221400*), photosystem I light-harvesting complex gene 5 (*Vigun09g238500*), cytochrome b6f complex subunit (petM) (*Vigun09g241500*), plastocyanin (petE) (*Vigun09g257300*) and Photosystem II reaction center PsbP family protein (*Vigun09g263400*), as well as members of the thioredoxin superfamily (*Vigun09g154700, Vigun09g167600, Vigun09g224600, Vigun09g238200 and Vigun09g256300*) and thioredoxin M-type 4 (*Vigun09g156800*).

Conclusions

In this work, we explored stress-induced responses of a range of related, rapidly measurable photosynthetic processes in a RIL population of cowpea lines. These responses reflect the genetically-controlled variations in control or regulation of photosynthesis. This approach is distinct from classically genetics, where mutations typically inactivate, typically, one or a few distinct enzymes in each genotype, leading to discrete loss of function phenotypes. Here, we may see combinations of effects that impact networks of processes are more likely to be adaptive.

Considering that the QTL regions in our study encompass hundreds of genes, we do not extensively explore the identities of specific, causative candidate polymorphisms. In some cases, it is possible to identify the causative genetic components that underlie QTL or GWAS effects (e.g. (Caicedo, Stinchcombe, Olsen, Schmitt & Purugganan 2004; Roux, Camilleri, Giancola, Brunel & Reboud 2005)), but these cases are relatively few considering the number of published studies on genetic variation and quantitative trait locus (QTL) mapping, partly because of the low resolution of the genetic maps of most diversity panels (Roff 2007; Miles & Wayne 2008; Baxter 2020). Nevertheless, even at lower resolution, such genomic associations can be used to guide plant breeding efforts, and may provide important leads for specific genetic components that can be tested in future work. Here, we identify several interesting candidates including structural and regulatory components of photosynthesis.

More importantly, the colocalization (or lack thereof) can be used to formulate and test scientific hypotheses, as we have demonstrated here, and thus give new insights into the processes that evolution has modulate physiological responses. This approach makes comparisons across genotype, emphasising genetically controlled differences, rather than the biophysical mechanisms per se. In other words, we observe how the genetic variations existing in a population "tweak" the mechanisms of photosynthesis. Key to this approach is the fact that each genotype in the population may have many combinations of smaller, quantitative, effects that add up or interact to achieve altered responses. The statistical analyses of associations between the genetic components and measured parameters can give insights into the processes that control particular phenotypes. By comparing these associations across phenotypes, we can get further insights into how genetic variations affect the connections among related processes, i.e., which processes are potentially mechanistically or genetically linked to others.

Analysis of our cowpea RIL using high time-resolved, high-throughput methods, points to a model where important genetic control at the levels of the redox states of Q_A and *pmf*, which governs the recombination reactions within PSII that can lead to singlet O_2 production. We predict that applying these methods to diversity panels from diverse species will reveal additional mechanisms of adaptation and will guide the breeding and engineering of photosynthesis for higher, more climate resilient productivity.

Author contributions

DH and DMK conceived the idea. DH conducted the experiments and wrote the initial draft of the manuscript. DH, AK, JAC, NF, IO-B and DMK interpreted data. PAR and BLH developed and genotype the RIL populations used and supported the SNP marker information and linkage map. All helped with data analyses and writing and revision of the manuscript. All authors approve of the final manuscript.

by MSU AgBioResearch program.

Bibliography

Allen D.J. & Ort D.R. (2001) Impacts of chilling temperatures on photosynthesis in warm-climate plants. *Trends in Plant Science* **6**, 36–42.

Aro E.-M., Virgin I. & Andersson B. (1993) Photoinhibition of photosystem II. Inactivation, protein damage and turnover. *Biochimica et Biophysica Acta (BBA)-Bioenergetics* **1143**, 113–134.

Avenson T.J., Cruz J.A., Kanazawa A. & Kramer D.M. (2005a) Regulating the proton budget of higher plant photosynthesis. *Proceedings of the National Academy of Sciences of the United States of America* **102**, 9709–9713.

Avenson T.J., Kanazawa A., Cruz J.A., Takizawa K., Ettinger W.E. & Kramer D.M. (2005b) Integrating the proton circuit into photosynthesis: progress and challenges. *Plant, Cell & Environment* **28**, 97–109.

Baker N.R., Harbinson J. & Kramer D.M. (2007) Determining the limitations and regulation of photosynthetic energy transduction in leaves. *Plant, Cell & Environment* **30**, 1107–1125.

Baker N.R. & Oxborough K. (2004) Chlorophyll fluorescence as a probe of photosynthetic productivity. In *Chlorophyll a Fluorescence*. pp. 65–82. Springer.

Baxter I. (2020) We aren't good at picking candidate genes, and it's slowing us down. *Current Opinion in Plant Biology* **54**, 57–60.

Boukar O., Fatokun C.A., Huynh B.-L., Roberts P.A. & Close T.J. (2016) Genomic tools in cowpea breeding programs: status and perspectives. *Frontiers in plant science* **7**, 757.

Broman K.W. & Sen S. (2009) *A Guide to QTL Mapping with R/qtl*. Springer New York, New York, NY.

Broman K.W. (2001) Review of statistical methods for QTL mapping in experimental crosses. *Lab animal* **30**, 44–52.

Caicedo A.L., Stinchcombe J.R., Olsen K.M., Schmitt J. & Purugganan M.D. (2004) Epistatic interaction between Arabidopsis FRI and FLC flowering time genes generates a latitudinal cline in a life history trait. *Proceedings of the National Academy of Sciences of the United States of America* **101**, 15670–15675.

Chassin Y., Kapri-Pardes E., Sinvany G., Arad T. & Adam Z. (2002) Expression and characterization of the thylakoid lumen protease DegP1 from Arabidopsis. *Plant Physiology* **130**, 857–864.

Chow W.S. & Hope A.B. (2004) Kinetics of reactions around the cytochrome bf complex studied in intact leaf disks. *Photosynthesis Research* **81**, 153–163.

Collin V., Issakidis-Bourguet E., Marchand C., Hirasawa M., Lancelin J.-M., Knaff D.B. & Miginiac-Maslow M. (2003) The Arabidopsis plastidial thioredoxins: new functions and new insights into specificity. *The Journal of Biological Chemistry* **278**, 23747–23752.

Cruz J.A., Avenson T.J., Kanazawa A., Takizawa K., Edwards G.E. & Kramer D.M. (2005) Plasticity in light reactions of photosynthesis for energy production and photoprotection. *Journal of Experimental Botany* **56**, 395–406.

Cruz J.A., Savage L.J., Zegarac R., Hall C.C., Satoh-Cruz M., Davis G.A., … Kramer D.M. (2016) Dynamic environmental photosynthetic imaging reveals emergent phenotypes. *Cell Systems* **2**, 365–377.

Davis G.A., Kanazawa A., Schöttler M.A., Kohzuma K., Froehlich J.E., Rutherford A.W., … Kramer D.M. (2016) Limitations to photosynthesis by proton motive force-induced photosystem II photodamage. *eLife* **5**.

Ehlers J.D., Hall A.E., Patel P.N., Roberts P.A. & Matthews W.C. (2000) Registration of California blackeye cowpea. *Crop Science* **40**, 854–854.

Fisher N., Bricker T.M. & Kramer D.M. (2019) Regulation of photosynthetic cyclic electron flow pathways

by adenylate status in higher plant chloroplasts. *Biochimica et biophysica acta. Bioenergetics* **1860**, 148081.

Flood P.J., Harbinson J. & Aarts M.G.M. (2011) Natural genetic variation in plant photosynthesis. *Trends in Plant Science* **16**, 327–335.

Geigenberger P., Thormählen I., Daloso D.M. & Fernie A.R. (2017) The unprecedented versatility of the plant thioredoxin system. *Trends in Plant Science* **22**, 249–262.

Gu L., Hanson P.J., Post W.M., Kaiser D.P., Yang B., Nemani R., … Meyers T. (2008) The 2007 eastern US spring freeze: increased cold damage in a warming world? *Bioscience* **58**, 253–262.

Herbert T.J. (1992) Geometry of heliotropic and nyctinastic leaf movements. *American Journal of Botany* **79**, 547–550.

Huang W., Zhang J.-L., Zhang S.-B. & Hu H. (2014) Evidence for the regulation of leaf movement by photosystem II activity. *Environmental and experimental botany* **107**, 167–172.

Huang W., Zhang S.-B. & Cao K.-F. (2012) Evidence for leaf fold to remedy the deficiency of physiological photoprotection for photosystem II. *Photosynthesis Research* **110**, 185–191.

Huner N.P.A., Öquist G. & Sarhan F. (1998) Energy balance and acclimation to light and cold. *Trends in Plant Science* **3**, 224–230.

Hutchison R.S., Groom Q. & Ort D.R. (2000) Differential effects of chilling-induced photooxidation on the redox regulation of photosynthetic enzymes. *Biochemistry* **39**, 6679–6688.

Huynh B.-L., Ehlers J.D., Huang B.E., Muñoz-Amatriaín M., Lonardi S., Santos J.R.P., … Roberts P.A. (2018) A multi-parent advanced generation inter-cross (MAGIC) population for genetic analysis and improvement of cowpea (Vigna unguiculata L. Walp.). *The Plant Journal: for Cell and Molecular Biology* **93**, 1129–1142.

Huynh B.-L., Matthews W.C., Ehlers J.D., Lucas M.R., Santos J.R.P., Ndeve A., … Roberts P.A. (2016) A major QTL corresponding to the Rk locus for resistance to root-knot nematodes in cowpea (Vigna unguiculata L. Walp.). *TAG. Theoretical and Applied Genetics. Theoretische und Angewandte Genetik* **129**, 87–95.

Ivanov A.G., Rosso D., Savitch L.V., Stachula P., Rosembert M., Oquist G., … Hüner N.P.A. (2012) Implications of alternative electron sinks in increased resistance of PSII and PSI photochemistry to high light stress in cold-acclimated Arabidopsis thaliana. *Photosynthesis research* **113**, 191–206.

Jansen R.C. (2004) Quantitative trait loci in inbred lines. In *Handbook of statistical genetics*. (eds D.J. Balding, M. Bishop & C. Cannings), John Wiley & Sons, Ltd, Chichester.

Kanazawa A. & Kramer D.M. (2002) In vivo modulation of nonphotochemical exciton quenching (NPQ) by regulation of the chloroplast ATP synthase. *Proceedings of the National Academy of Sciences of the United States of America* **99**, 12789–12794.

Kanazawa A., Ostendorf E., Kohzuma K., Hoh D., Strand D.D., Sato-Cruz M., … Kramer D.M. (2017) Chloroplast ATP synthase modulation of the thylakoid proton motive force: implications for photosystem I and photosystem II photoprotection. *Frontiers in plant science* **8**, 719.

Kapri-Pardes E., Naveh L. & Adam Z. (2007) The thylakoid lumen protease Deg1 is involved in the repair of photosystem II from photoinhibition in Arabidopsis. *The Plant Cell* **19**, 1039–1047.

Kramer D.M., Avenson T.J. & Edwards G.E. (2004) Dynamic flexibility in the light reactions of photosynthesis governed by both electron and proton transfer reactions. *Trends in Plant Science* **9**, 349–357.

Kuhlgert S., Austic G., Zegarac R., Osei-Bonsu I., Hoh D., Chilvers M.I., … Kramer D.M. (2016) MultispeQ Beta: a tool for large-scale plant phenotyping connected to the open PhotosynQ network. *Royal Society Open Science* **3**, 160592.

Lonardi S., Muñoz-Amatriaín M., Liang Q., Shu S., Wanamaker S.I., Lo S., … Close T.J. (2019) The genome of cowpea (Vigna unguiculata [L.] Walp.). *The Plant Journal: for Cell and Molecular Biology* **98**, 767–782.

Long S.P., Zhu X.-G., Naidu S.L. & Ort D.R. (2006) Can improvement in photosynthesis increase crop

yields? *Plant, Cell & Environment* **29**, 315–330.

Lucas M.R., Diop N.-N., Wanamaker S., Ehlers J.D., Roberts P.A. & Close T.J. (2011) Cowpea–Soybean Synteny Clarified through an Improved Genetic Map. *The Plant Genome Journal* **4**, 218.

Maeda K., Finnie C. & Svensson B. (2004) Cy5 maleimide labelling for sensitive detection of free thiols in native protein extracts: identification of seed proteins targeted by barley thioredoxin h isoforms. *The Biochemical Journal* **378**, 497–507.

Marx C., Wong J.H. & Buchanan B.B. (2003) Thioredoxin and germinating barley: targets and protein redox changes. *Planta* **216**, 454–460.

Meng L., Li H., Zhang L. & Wang J. (2015) QTL IciMapping: Integrated software for genetic linkage map construction and quantitative trait locus mapping in biparental populations. *The Crop journal* **3**, 269–283.

Miles C.M. & Wayne M. (2008) Quantitative trait locus (QTL) analysis. *Nature Education 1 (1)* **208**.

Moon B.Y., Higashi S., Gombos Z. & Murata N. (1995) Unsaturation of the membrane lipids of chloroplasts stabilizes the photosynthetic machinery against low-temperature photoinhibition in transgenic tobacco plants. *Proceedings of the National Academy of Sciences of the United States of America* **92**, 6219–6223.

Muchero W., Diop N.N., Bhat P.R., Fenton R.D., Wanamaker S., Pottorff M., … Close T.J. (2009) A consensus genetic map of cowpea [Vigna unguiculata (L) Walp.] and synteny based on EST-derived SNPs. *Proceedings of the National Academy of Sciences of the United States of America* **106**, 18159–18164.

Muchero W., Roberts P.A., Diop N.N., Drabo I., Cisse N., Close T.J., … Ehlers J.D. (2013) Genetic architecture of delayed senescence, biomass, and grain yield under drought stress in cowpea. *Plos One* **8**, e70041.

Murata N., Takahashi S., Nishiyama Y. & Allakhverdiev S.I. (2007) Photoinhibition of photosystem II under environmental stress. *Biochimica et Biophysica Acta* **1767**, 414–421.

ORT D.R. (2002) Chilling-induced limitations on photosynthesis in warm climate plants: contrasting mechanisms. *Environment Control in Biology* **40**, 7–18.

Ortiz, D., Hu, J., and Salas Fernandez, M.G. (2017). Genetic architecture of photosynthesis in Sorghum bicolor under non-stress and cold stress conditions. Journal of experimental botany **68**: 4545–4557.

Park J.H., Lee E.S., Chae H.B., Paeng S.K., Wi S.D., Bae S.B., … Lee S.Y. (2021) Disulfide reductase activity of thioredoxin-h2 imparts cold tolerance in Arabidopsis. *Biochemical and Biophysical Research Communications* **568**, 124–130.

Prinzenberg A.E., Campos-Dominguez L., Kruijer W., Harbinson J. & Aarts M.G.M. (2020) Natural variation of photosynthetic efficiency in Arabidopsis thaliana accessions under low temperature conditions. *Plant, Cell & Environment* **43**, 2000–2013.

Raines C.A. (2011) Increasing photosynthetic carbon assimilation in C3 plants to improve crop yield: current and future strategies. *Plant Physiology* **155**, 36–42.

Roff D.A. (2007) A centennial celebration for quantitative genetics. *Evolution* **61**, 1017–1032.

Rouhier N., Gelhaye E., Sautiere P.E., Brun A., Laurent P., Tagu D., … Jacquot J.P. (2001) Isolation and characterization of a new peroxiredoxin from poplar sieve tubes that uses either glutaredoxin or thioredoxin as a proton donor. *Plant Physiology* **127**, 1299–1309.

Roux F., Camilleri C., Giancola S., Brunel D. & Reboud X. (2005) Epistatic interactions among herbicide resistances in Arabidopsis thaliana: the fitness cost of multiresistance. *Genetics* **171**, 1277–1288.

Sassenrath G.F., Ort D.R. & Portis Jr A.R. (1990) Impaired reductive activation of stromal bisphosphatases in tomato leaves following low-temperature exposure at high light. *Archives of Biochemistry and Biophysics* **282**, 302–308.

Schürmann P. & Jacquot J.P. (2000) Plant thioredoxin systems revisited. *Annual review of plant biology* **51**, 371–400.

Sonoike K. (1996) Photoinhibition of photosystem I: its physiological significance in the chilling sensitivity of plants. *Plant and Cell Physiology* **37**, 239–247.

Takagi D., Takumi S., Hashiguchi M., Sejima T. & Miyake C. (2016) Superoxide and Singlet Oxygen Produced within the Thylakoid Membranes Both Cause Photosystem I Photoinhibition. *Plant Physiology* **171**, 1626–1634.

Takizawa K., Kanazawa A., Kramer D.M., (2008) Depletion of stromal P(i) induces high "energy-dependent" antenna exciton quenching (q(E)) by decreasing proton conductivity at CF(O)-CF(1) ATP synthase. *Plant Cell Environ* **31**, 235–43.

Telfer A. (2014) Singlet oxygen production by PSII under light stress: mechanism, detection and the protective role of β-carotene. *Plant & Cell Physiology* **55**, 1216–1223.

Tietz S., Hall C.C., Cruz J.A. & Kramer D.M. (2017) NPQ(T) : a chlorophyll fluorescence parameter for rapid estimation and imaging of non-photochemical quenching of excitons in photosystem-II-associated antenna complexes. *Plant, Cell & Environment* **40**, 1243–1255.

Tikkanen M., Grieco M., Nurmi M., Rantala M., Suorsa M. & Aro E.-M. (2012) Regulation of the photosynthetic apparatus under fluctuating growth light. *Philosophical Transactions of the Royal Society of London. Series B, Biological Sciences* **367**, 3486–3493.

Tyystjärvi E. & Aro E.M. (1996) The rate constant of photoinhibition, measured in lincomycin-treated leaves, is directly proportional to light intensity. *Proceedings of the National Academy of Sciences of the United States of America* **93**, 2213–2218.

Van Os H., Stam P., Visser R.G.F. & Van Eck H.J. (2005) RECORD: a novel method for ordering loci on a genetic linkage map. *TAG. Theoretical and Applied Genetics. Theoretische und Angewandte Genetik* **112**, 30–40.

Yang J.T., Preiser A.L., Li Z., Weise S.E. & Sharkey T.D. (2016) Triose phosphate use limitation of photosynthesis: short-term and long-term effects. *Planta* **243**, 687–698.

Yoshida K., Matsuoka Y., Hara S., Konno H. & Hisabori T. (2014) Distinct redox behaviors of chloroplast thiol enzymes and their relationships with photosynthetic electron transport in Arabidopsis thaliana. *Plant & Cell Physiology* **55**, 1415–1425.

Zack G.W., Rogers W.E. & Latt S.A. (1977) Automatic measurement of sister chromatid exchange frequency. *The Journal of Histochemistry and Cytochemistry* **25**, 741–753.

Zelitch I. (1982) The close relationship between net photosynthesis and crop yield. *Bioscience* **32**, 796–802.